



Design and implementation of analysis pipeline for single cell type proteomics data

presenting ProteoScanR & Proteomics Workbench

Lukas Gamp
01630003

In partial fulfillment of the requirement
for the degree of MSc
in Bioinformatics

July 2023

Main Supervisor: Dr. DI(FH) Gerhard Duernberger

External Supervisor: Assoc. Prof. Ujjwal Neogi, M.Sc. PhD

Second examiner: FH-Prof. Dr. Alexandra Graf

Abstract

With the growing prominence of single-cell techniques across various omics fields, there is a pressing need to develop a standardized pipeline for proteomics data in the realm of systems biology. Unlike DNA sequencing and RNA sequencing, proteomics analysis via mass spectrometry incurs high costs in terms of labor and equipment. Additionally, commercially available software solutions often come with hefty price tags and limited transparency regarding the underlying methods employed. However, MaxQuant (Cox & Mann 2008) presents a promising alternative, complemented by the flexibility using the R programming language. Introducing ProteoScanR, a state-of-the-art proteomics pipeline integrated into the user-friendly Proteomics Workbench interface. Guided by SCoPE2 (Specht et al. 2021, Petelski et al. 2021, Vanderaa & Gatto 2021), the development process of ProteoScanR was thoroughly tested and validated using both bulk and single-cell mass spectrometry data sets. The pipeline implementation in the Proteomics Workbench leverages the power of an interactive environment built in R Shiny, empowering users to discover valuable insights for their specific data set. Within the interactive environment, users have the flexibility to customize cutoffs and thresholds for quality control, as well as employ various approaches for data transformation, normalization, missing value imputation, and batch correction. ProteoScanR and the Proteomics Workbench served as a valuable tool in guiding the identification of significantly expressed proteins in cells under study. Subsequently, the pathway enrichment analysis provided additional biological contexts for a comprehensive understanding of their functional implications. The master thesis project serves as a foundation for future advancements in the field of single-cell proteomics. Moreover, the codebase has been designed with robustness and scalability in mind, ensuring ease of maintenance and future expansion of the application.

<https://github.com/Lukas67/ProteoScanR>

Contents

1	Introduction	2
1.1	From the Central Dogma of Molecular Biology to Omics and Systems Biology	2
1.2	Proteomics	2
1.2.1	Bulk proteomics	3
1.2.2	Single-cell type proteomics	3
1.2.3	Single-cell proteomics	4
1.3	Capturing the proteome	5
1.3.1	Mass Spectrometry	6
1.3.2	Data processing	8
1.3.3	Downstream analysis	10
2	Materials and Methods	12
2.1	Wetlab - Materials and Methods	12
2.1.1	Celltypes	12
2.1.2	Digestion	12
2.1.3	Labeling	12
2.1.4	Pooling	12
2.1.5	Liquid chromatography	12
2.1.6	Mass Spectrometry	13
2.2	Drylab - Computational methods	13
2.2.1	Hardware	13
2.2.2	Data-acquisition and raw-file analysis	13
2.2.3	Processing the data	15
2.2.4	Object oriented programming	15
2.2.5	Zero values	15

2.2.6	Exclude reverse matches/contaminants	16
2.2.7	Filter according to precursor ion fraction (PIF)	16
2.2.8	Filter by q-value	16
2.2.9	Peptide spectrum match (PSM) aggregation to peptides	17
2.2.10	Join assays	17
2.2.11	Calculate median reporter ion intensity (RI) and filter	17
2.2.12	Calculate median coefficient of variation (CV) and filter	17
2.2.13	Remove peptides with high missing rate	18
2.2.14	Aggregation of peptides to proteins	18
2.2.15	Transformation of protein expression data	18
2.2.16	Normalization	19
2.2.17	Missing value handling	21
2.2.18	Batch correction	22
2.2.19	Dimensionality reduction	23
2.2.20	Validation of the methods applied to the dataset	25
2.2.21	Statistics	26
2.2.22	Protein set enrichment analysis	28
3	Results	31
4	Discussion	56
4.1	Interactive pipeline	56
4.2	Mutual Information	57
4.3	Reporter ion intensity	57
4.4	Median coefficient of variation	57
4.5	Feature-wise plot	58
4.6	Statistics module	58

4.7	Enrichment	59
4.8	Limitations	60
4.9	Future perspectives	61
4.9.1	Clustering for stratification of cells.	61
4.9.2	Machine learning	64
5	Conclusion	66
6	Bibliography	68
7	Appendix	74
7.1	Wet lab	74
7.1.1	Cells sorting protocol	74
7.1.2	Digestion protocol	74
7.1.3	Labeling protocol	74
7.1.4	Pooling protocol	75
7.2	Dry lab	75
7.2.1	R-version info	75
List of Figures		80

Acknowledgements

In addition to my faithful feline companion, Apollo, who took care of my place in Austria while I was working on this project in Stockholm, I am deeply grateful to all the members of Ujjwal Neogi's research group.

Their unwavering guidance and support throughout this project have been truly invaluable, and I am profoundly thankful for their expertise and assistance.

1 Introduction

1.1 From the Central Dogma of Molecular Biology to Omics and Systems Biology

Before the initial exploration of molecular biology, the processes of life were roughly inferred and not well understood. The central dogma of molecular biology serves as the cornerstone of biological processes, providing a framework for understanding how genetic information is converted into functional proteins. This framework consists of two major processes: transcription, which converts DNA into RNA, and translation, which converts RNA into functional proteins. Between these processes, molecular-level regulation occurs through chemical adaptations. This regulation is crucial for biological organisms to efficiently produce their genetic products, known as proteins. Crick's formulation of the central dogma has guided research in molecular biology for over 60 years (Cobb 2017). Over the past six decades, researchers have explored various aspects of this principle, collectively referred to as "omics," to comprehensively analyze biomolecules in diverse contexts. Omics research has emerged as an approach to study biomolecules and their interactions within biological systems comprehensively. Omics encompasses various fields, including genomics, transcriptomics, proteomics, and metabolomics, with each field focusing on a specific class of biomolecules. By analyzing multiple layers of omics data, researchers can gain a holistic view of biological processes, uncover regulatory mechanisms, and identify key players in complex biological networks using computational methods. Systems biology takes a quantitative approach to investigate the interactions, dynamics, and emergent properties of biomolecular networks. Biological systems are imagined as complex, multi-layer networks, with the ensemble of proteins, known as the proteome, playing a critical role in this interactive structure. Proteins have various functions, such as providing structural integrity, catalyzing chemical reactions, and regulating cellular functions (Karahalil 2016)

1.2 Proteomics

The central dogma of molecular biology offers insights not only at the level of individual terms but also provides a hierarchical understanding of biology. Hierarchical organization is the underlying principle in all topics of biology. Proteins exhibit hierarchical structures that contribute to their functionality. At the primary structure level, proteins are composed of smaller building blocks called amino acids. Combining them results in the protein secondary structure such as alpha helix and beta sheet. These secondary structures further assemble to create higher-order tertiary structures, which

represent specific domains within the protein. Finally, the quaternary structure describes the functional state of the protein as a whole at a given time. Proteomics is a comprehensive approach that investigates the complete protein composition of a specimen, aiming to understand the intricate biological network it represents. For instance if pathogens interact with cells of an organism a cascade of biochemical reactions takes place. These reactions influence the outcome of the cellular proteome in regards of localization, abundance, post-translational modifications (Beltran et al. 2017). By studying the proteome, we can gain a comprehensive understanding of the hierarchical organization and functional dynamics of biological processes.

1.2.1 Bulk proteomics

Higher organisms are composed of specialized cells organized into tissues, such as skin, muscle, and blood. Each tissue consists of cells with specific functions, resulting in variations in protein expression. Bulk proteomics is a technique used to analyze the protein composition of a tissue sample, which contains all types of cells present in that particular tissue. This approach finds valuable applications for instance in oncology, where it can provide insights into the protein profile of a tumor. By studying oncogenic biomarkers and expression patterns, this knowledge can contribute to the development of screening methods and the customization of treatments. Additionally, bulk proteomics can aid in identifying the progression of tumor development (Kwon et al. 2021). Bulk analysis expression profiles provide scientists with an average protein abundance across all cells in a sample, offering a comprehensive view of protein expression. Additionally, compared to single-cell methods, bulk samples typically contain a greater number of proteins. In fact the expanded library can be used to validate the performance of single-cell type and single-cell proteomics methods and bioinformatics pipeline (Schoof et al. 2021). However, in this type of analysis, the precise properties of individual cell types can only be inferred and remain obscured.

1.2.2 Single-cell type proteomics

Taking tissue samples can lead to an averaging effect across the entire cellular ensemble, making it difficult to discern specific cell types. To overcome this limitation, cell sorting techniques such as fluorescence-activated cell sorting (FACS), magnetic-activated cell sorting (MACS), and buoyancy-activated cell sorting (BACS) are employed (Liou et al. 2015). These techniques primarily rely on the detection of surface proteins on cells and the specific binding of antibodies to these proteins. Auto-fluorescence is observed in certain cells, wherein they possess the capability to emit a

light signal when stimulated, and this emission can be used to sort them accordingly. However auto-fluorescence can lack of accuracy as shown in studies indicating the effect of laboratory gloves on cellular samples (Philpott et al. 2017). On the other side antibodies, typically derived from the immune system of other species, bind to antigens in a highly specific lock-and-key manner. Antibodies are widely used in molecular biology and find applications in cell isolation. Depending on the desired application, the antibodies can be labeled with fluorescent markers (FACS), magnetic beads (MACS), or biotin (BACS). These methods have varying technical requirements, with flow cytometers being the most complex and costly. In MACS, magnetic beads are used to isolate cells from a solution by utilizing a magnet. However, mechanical forces involved in MACS can potentially damage the cells. BACS, a method developed in 2015, employs microbubbles to carry the antibodies for cellular isolation. The method showed improvements compared to MACS in regards of viability after sorting. It is important to note that FACS is considered the gold standard for validating the effectiveness of MACS and BACS due to its high purity and yield. FACS was used in the validation of these two methods (Liou et al. 2015, Sutermaster & Darling 2019). Single-cell type proteomics reflects the protein ensemble of a specific cell type at a particular time, providing a focused perspective on the studied field compared to bulk methods (Maes et al. 2020).

1.2.3 Single-cell proteomics

Cell sorting techniques primarily rely on extracellular proteins to identify and separate different cell types. However, the intracellular content of cells can still exhibit variability in experiments. Single-cell proteomics (SCP) addresses this limitation by providing a snapshot of the underlying processes within an individual cell, eliminating this variability and allowing for the elucidation of the principles of cell type behavior, such as differentiation. Differentiation, a critical process in various biological systems such as the immune system, involves the acquisition of specialized functions by specific cell types (Fang et al. 2018). Investigating differentiation in multiple cells can be challenging due to the inherent heterogeneity during the initiation of this process. However, by analyzing one cell at a time and observing it throughout the differentiation process, researchers can capture the complete trajectory of differentiation at a single-cell level. This approach provides valuable insights into the dynamic changes occurring within cells during differentiation. In 2021, Specht et al. developed the SCoPE2 sample preparation and analysis pipeline, performing macrophage-monocyte differentiation experiments (Specht et al. 2021). This pipeline streamlined the sample preparation process, reducing labor time and providing a reference model for subsequent SCP projects. SCP has proven to be a powerful tool for studying a wide range of biological phenomena,

including drug responses, infectious diseases, and organism development. Over the past decade, single-cell techniques, including SCP, have become indispensable tools for the global research community (Minakshi et al. 2019).

1.3 Capturing the proteome

An early approach of qualitative analysis of the cellular proteome involved labeling with fluorescent antibodies and imaging. The major disadvantage of this technique was the limitation to only stain a few proteins per cell and the requirement of a-priori knowledge of the protein to analyze. For quantification, procedures such as Western blots, immunoassays or cytometry by time of flight (CyTOF) have been used. Challenges are the ability to permeate cells, accessibility and binding of the epitope and the creation of specific antibodies for a given protein (Budnik et al. 2018). Early quantitative methods in molecular biology, measuring the entire protein concentration, were assays like the UV-vis-, Bradford- and/or bicinchoninic-acid-assay. These methods are still in use to obtain total concentration for sample preparation. Another quantitative technique involved RNA-sequencing. RNAseq refers to the task of examining the transcriptome of bulk tissue sample with deep-sequencing technologies. RNA in a sample includes mRNAs, non-coding RNAs, and small RNAs. One of the main disadvantages is, that the mapping relies on the knowledge of the DNA sequence of the observed organism (reference genome) (Wang et al. 2009). Another disadvantage is, that the amount of protein translated from the determined mRNA can only be estimated (Gygi et al. 1999). However, today these predictions can be done with computational methods such as LASSO and the accuracy of the estimate highly depends on selection and validation of this method (Magnusson et al. 2022). When observing the protein ensemble of a cellular environment with a top-down approach like DNaseq or RNAseq, the characteristics (e.g. post-translational modifications or charge) and local concentration of the proteins remain hidden. The cause of this phenomenon is that only a fraction of the DNA is transcribed into mRNA and not all mRNA is further translated into protein. Furthermore multiple proteins can be derived from a single DNA-sequence with alternative splicing and different proteins coming from non related sequences acting like building blocks can form protein complexes and/or Protein-RNA complexes. Cells are highly efficient and do not waste energy by producing obsolete proteins, moreover the degradation of proteins in the proteasome is an important energy recovery mechanism (TANAKA 2009). A bottom-up strategy can elucidate these properties of the protein ensemble at a given time leading to proteomics. When studying impact of an external signal or stressor to a cell the abundance and properties of a protein or protein-ensemble can enlighten the underlying pathway leading to a biological response. Since

some proteins do not even function before post-translational modifications (PTMs) happen, a knowledge about these can be crucial for further studies. Mass spectrometry (MS) fusions the advantages of the above mentioned techniques, because it combines the specificity of qualitative assays which are even able to sense (PTMs) with the quantitative accuracy of protein concentration assays. Furthermore MS does not require any a-priori knowledge of the protein ensemble of the specimen, making it the method of choice for untargeted approaches.

1.3.1 Mass Spectrometry

Mass spectrometry enables qualitative and quantitative analysis of the entire repertoire of a biological sample. Mass spectrometers measure the mass to charge ratio (m/z) of a particle from a fragmented larger molecule. This is achieved by a physical procedure done with a device which is made of three major components: the ion source, an analyzer, and a detector. The ion sources charges molecules and accelerate them through a magnetic field. The analyzer separates particles according to their mass to charge ratio and the detector senses charged particles and amplifies their signal (Parker et al. 2010). However before acquiring any data, sample preparation and pre-processing is required. After sample preparation the first step involves tryptic digestion. It is a widely used technique in shotgun proteomics and involves the enzymatic cleavage of proteins into smaller peptides using the protease enzyme trypsin. The process known as proteolysis takes place in multiple parts of multi cellular organisms and was firstly detected in the small intestine digesting proteins (Wang et al. 2008). The enzyme cleaves specifically at the carboxyl side of arginine and lysin residues. Afterwards a charge remains on the residues making them detectable for the mass spectrometer. It is proven that proteins which are digested to the limit, meaning no further proteolysis can be induced, provide the best results in such bottom up approaches (Brownridge & Beynon 2011, Ünige A. Laskay et al. 2013).

To observe multiple samples in one run, labeling is needed to identify each sample within a batch. Since mass spectrometry is not a quantitative technique by itself, the peak height or area does not reflect the abundance of a peptide. Physicochemical properties of the peptides can change the ionization efficiency and detectability of the target. However, when comparing the same analyte between multiple runs of labeled peptides, differences in the reporter ion intensity reflect the abundance of those. Labels should be chosen to change solely the mass of the sample and to not affect folding or other inherent properties of the peptide. The two techniques for labeling peptides are metabolic labeling and isobaric labling. In metabolic labeling the cells were fed with aminoacids containing heavy isotopes, it is the method of choice in order to label peptides at the earliest possible level. This atoms can be heavy nitrogen in aminoacids or salts in fertilizer for plants (A. & Demmers

2012). Mass shifts are proportional to the isotopes incorporated during biomass production and are visible after proteolytic cleavage. Stable isotope labeling in cell culture (SILAC) was presented in the early 2000s. This method used heavy aminoacid enriched media to feed cells, in order to quantitatively analyze expression profiles. The limitation of this method is, that it can only be applied to a human cell culture (*in vitro*) or to model organisms (*in vivo*). Isobaric labeling solely applies to *in vitro* techniques, with TMT and iTRAQ. The data analyzed by ProteoScanR primarily utilized TMT tags. Tandem mass tag (TMT) reagents enable differentiation of multiple samples in a single mass spectrometry (MS) run. Each sample is individually labeled with TMT reagents and then pooled together, this procedure is called multiplexing. TMTs have the same charge and differ only by their isotopic masses, the peaks observed for each sample are called reporter ions (RI). Each RI and sample is interpreted as one channel in downstream analysis. This technique allows for the identification, enrichment, and quantification of low-abundance peptide ions, which is particularly valuable in single-cell techniques. With this technique it is possible to quantify proteins and filter low abundant proteins from background noise. However, a drawback of isobaric labeling is the presence of co-fragmentation signals in the spectrogram, which requires data normalization to remove unwanted contributions (Marx 2019, Budnik et al. 2018). Isotopic distribution in TMTs, reflecting the natural distribution, can be corrected during data acquisition by considering a defined spread in other channels. Single-cell proteomics by mass spectrometry (SCoPE-MS) uses isobaric labeling with a tandem mass tag (TMT) to enhance signal intensity of a protein species. Loading of a single-cell channel (SCC) with the right amount can be balanced to the protein concentration of a single cell (Ye et al. 2022).

Before ionization peptides need to be further separated according to their chemical properties, size or species by liquid chromatography (LC), because the number of peptide processed simultaneously by the MS device is limited. In the case of mass spectrometry, liquid chromatography especially high performance LC (HPLC) is the technique of choice and replaces the instrumentation-wise simpler technique gel electrophoresis. In HPLC the molecules elute through a narrow column with high pressures (50-350 bar), compared to LC where the separation is gravity dependent. Similar to gel electrophoresis molecules can be separated upon different chemical properties, depending on the type of the chromatography column. In a typical proteomics experiment peptides are separated with reversed phase chromatography (RPLC). The principle behind RPLC is a column with a nonpolar stationary phase which interacts with the nonpolar residues of the peptides. Peptides were fractionated according to their hydrophobicity (Pitt 2009).

To analyze a biological sample consisting of peptides in solution the liquid needs to be vaporized into

gas phase. Two techniques are capable of this procedure. Electrospray ionization (ESI) pushes the analyte through a capillary while applying an electric current to the liquid, vaporizing the sample to a charged aerosol. Peptides are further fragmented according to their chemical properties and can be further handled in the mass spectrometer. The fragmented peptides are now in charged droplets separated based on their surface charge, splitting further into smaller droplets until they reach the gas phase as ions. Two physical models describe the process from gas phase to ion called “The ion evaporation model” (IEM) and “The charge residue model” (CRM). In the ion evaporation model the droplets shrink by evaporation until ions are expelled (Iribarne 1976). The model had its limitation by explaining same evaporation rate constant among ions with different chemical properties. In the charge residue model the assumption of one molecule per droplet leads to an ionization rate constant, which is independent of the ion itself and relies solely on the generation of the droplet and the efficiency of the solvent (Wilm 2011).

Subsequently after the ionization peptides are accelerated through the magnetic field generated by the mass analyzer. Six general types of mass analyzers are available on the market, there are Quadropole, time of flight (TOF), magnetic sector, electrostatic sector, quadropole ion trap and ion cyclotron resonance -mass analyzer. The function of the mass analyzer is to separate ions based on their mass to charge ratio (m/z).

Before the signal of the separated ions can be obtained an optional subsequent step involves trapping the ions an electric and/or magnetic field in order to detect ions based on their (m/z) consecutively. Ion trapping enables the technique of coupled mass spectrometers, where ions were further fragmented by collision induced dissociation and analyzed subsequently. The detector transforms the impact energy of the ion into an electric signal, called spectrum which can be processed computationally.

1.3.2 Data processing

Given the high resolution of MS data, algorithms are employed to convert the raw signal into an interpretable form. Software packages like MaxQuant (Cox & Mann 2008) are commonly used to process the data, providing it for further analysis and statistical testing. Other software solutions include Proteome Discoverer by Thermo Fisher.

The data obtained from mass spectrometry has three dimensions: m/z ratio, intensity, and retention time. To separate peaks from each other, algorithms are used to identify local minima in the data. The centroid of each peak is determined by fitting a Gaussian peak shape, which can be interpreted

as locating the peaks of each m/z spectrum as a function of retention time. The centroid of a peak corresponds to an isotope.

In order to decipher the isotopic distribution of a biomolecule, MaxQuant employs a vertex-based approach. This process, referred to as de-isotoping, utilizes graph theory. It creates a vertex for each individual peak and connects them with their potential isotopic counterparts. This is achieved by determining the mass proportion of an average amino acid to its respective isotope using a concept known as averagine (Senko et al. 1995). By applying this procedure, the number of data points is reduced by a factor of ten, and each peak represents a small biomolecule.

The subsequent step in data acquisition involves the detection of labels for quantification purposes. Isotopic pairs of the label (such as N13, N14, N15) present in the tag or aminoacid are identified by convolving the two measured isotope patterns with the theoretical isotope patterns. Through an iterative process using a least-squares method, the best fit is determined, enabling the identification of the specific channel or sample.

The intensity-weighted average of the MS peak centroids, as described as 3D peak identification, corresponds to the mass of the peptide. The accuracy of mass measurements relies on the specific analyzer used. For an Orbitrap-type analyzer (which was used during this project), MaxQuant applies a correction value of 1 ppm (parts per million). Autocorrelation between centroids is accounted for by considering only well-identified peptides. Published data indicates that the mass precision within an MS experiment typically ranges around 10^{-7} (Wilschefski & Baxter 2019).

Each peptide is represented by its individual fingerprint in the MS spectrum, which is based on the sequence and modifications of amino acids. The m/z ratio of the amino acids can be calculated, and the resulting peaks are interpreted as an amino acid sequence. However, only peptide fragments are visible in the spectrum due to peptide fragmentation. To identify proteins, peptides are matched against a sequence database. Sequence databases are typically stored as .fasta files and can be downloaded from the UniProt database (www.uniprot.org). The availability of gene sequences in databases and the computational matching of peptides against those sequences enable the identification of alterations in a sample at the protein level. These alterations can rely on the sequence level or could be to post-translational modifications (PTMs) such as phosphorylations or methylations (Aebersold & Mann 2003). The peptide identification (P-) score reflects the goodness of fit between the data and the identified sequence in the database, taking into account the length of the peptide. This score is used to calculate the posterior error probability, which is then utilized to estimate the false discovery rate (FDR). The FDR calculation provides a measure of the rate at

which false identifications are expected in the dataset. Within the identified peptide groups, a “razor protein” refers to the protein with the highest number of ambiguously identified peptides.

Quantification is performed by considering only unique peptides for comparison. Posterior error probabilities, which represent the likelihood of the identified peptide being a random event, are multiplied together, and only distinct sequences with the highest scores are considered for further analysis. Various metrics that indicate the performance of the peptide search can be utilized in downstream analysis.

1.3.3 Downstream analysis

With advancements in mass spectrometry technology and computational methods, proteomic analysis has emerged as a powerful tool for investigating complex protein samples. However, analyzing proteomic data poses challenges in data processing, statistical analysis, and interpretation. This thesis aims to address these challenges by exploring computational methods for downstream analysis of proteomics data. The methods employed in this study will be thoroughly explained in the methods section, with a specific focus on developing an interactive environment equipped with a graphical user interface, called Proteomics Workbench. This user-friendly interface will enable researchers, including those with limited computational expertise, to navigate and comprehend the data effectively.

ProteoScanR comprises a series of steps to streamline the data. It begins with quality control measures at the peptide spectrum match level, involving the removal of contaminants and irrelevant channels. Significance levels of peptide spectrum matches serve as confidence thresholds for match selection. The data is then aggregated at the peptide level, followed by additional filtering procedures based on metrics such as reporter ion intensity, peptide coefficient of variation over razor proteins, and missing rates for peptides.

To derive meaningful biological insights from the dataset, statistical testing plays a crucial role. Selecting appropriate statistical tests and ensuring proper data transformation and normalization are essential steps. Many statistical methods rely on data distribution and require careful consideration to preserve the biological interpretation of the results. This thesis employs various transformation and normalization techniques, aiming to maintain data integrity and avoid biased interpretations. Additionally, an entropy-based visualization approach will provide users with a valuable tool for validating the computations and selected thresholds for the filtering steps.

Handling missing values poses further challenges in the pipeline development since a missing signal for a peptide results in a missing protein, which is highly unlikely in a biological context. Several

options for missing value handling will be included and thoroughly explained in the methods section.

Dimensionality reduction and visualization techniques are widely used to cluster data. In this project, multiple approaches will be utilized, and users will have the ability to visually and interactively observe the data.

It is important to acknowledge that downstream analysis in proteomics lacks a standardized approach, and the selection of computational methods depends on the specific dataset and research objectives. Furthermore, statistical analysis and the interpretation of biological meaning often present misconceptions that need to be addressed. For instance, batch correction, a commonly practiced method, has been overestimated in numerous studies, leading to misleading results (Nygaard et al. 2016). This thesis aims to contribute to the field by providing researchers with a comprehensive understanding of computational methods in proteomics analysis and their application in an interactive environment.

2 Materials and Methods

2.1 Wetlab - Materials and Methods

For testing and development of the ProteoScanR pipeline the following materials and methods were performed. For the sample preparation protocol see appendix.

2.1.1 Celltypes

Macrophages from 12 healthy donors and 12 HIV patients with metabolic syndrome and 12 HIV patients without metabolic syndrome. Cell sorting was performed with FACS Aria Fusion (BD Biosciences).

2.1.2 Digestion

Protein digestion was performed using trypsin (Promega, Madison, WA) buffered in Triethylammonium bicarbonate buffer (TEAB). Reagents were handled with MANTIS automatic dispenser (Formulatrix, Bedford, MA).

2.1.3 Labeling

Samples of test dataset were labeled with 12-plex TMTpro (Thermo Fisher) in anhydrous acetonitril (ACN) solution.

2.1.4 Pooling

Carrier proteome was added to the 36 TMTpro sets before pooling sample types for each of the 36 MS-runs.

2.1.5 Liquid chromatography

In order to separate peptides according to their chemical properties, size or species a liquid chromatography (LC) is recommended before ionization. For the reference data used for developing the pipeline the following instrumentation was used. EASY-Spray™ HPLC column, ES802A, 2 μm \times 75 μm ID \times 250 mm (ThermoFisher Scientific) Acclaim PepMap trap column, 2 μm \times 75 μm ID \times 2 cm (ThermoFisher Scientific)

2.1.6 Mass Spectrometry

2.1.6.1 Ionization For the reference data ESI ionization was used.

2.1.6.2 Mass spectrometer For the reference data used for developing the pipeline an OrbitrapTM FusionTM LumosTM tribrid mass spectrometer (ThermoFisher Scientific) was used. The instrumentation uses two subsequent runs in the analyzer (=Orbitrap) to increase mass accuracy.

2.2 Drylab - Computational methods

2.2.1 Hardware

Lenovo Laptop X360 with: Intel(R) Core(TM) i5-6200U CPU @ 2.30GHz 8 GB RAM

2.2.2 Data-acquisition and raw-file analysis

For the data-acquisition Thermo Fisher acquisition software was used. Raw-file analysis of the data was done with MaxQuantCmd 2.2.0.0 (Cox & Mann 2008). The default settings were used. TMTpro labels were corrected according to the isotopical distribution of the Lot-number provided by Thermo Fisher.

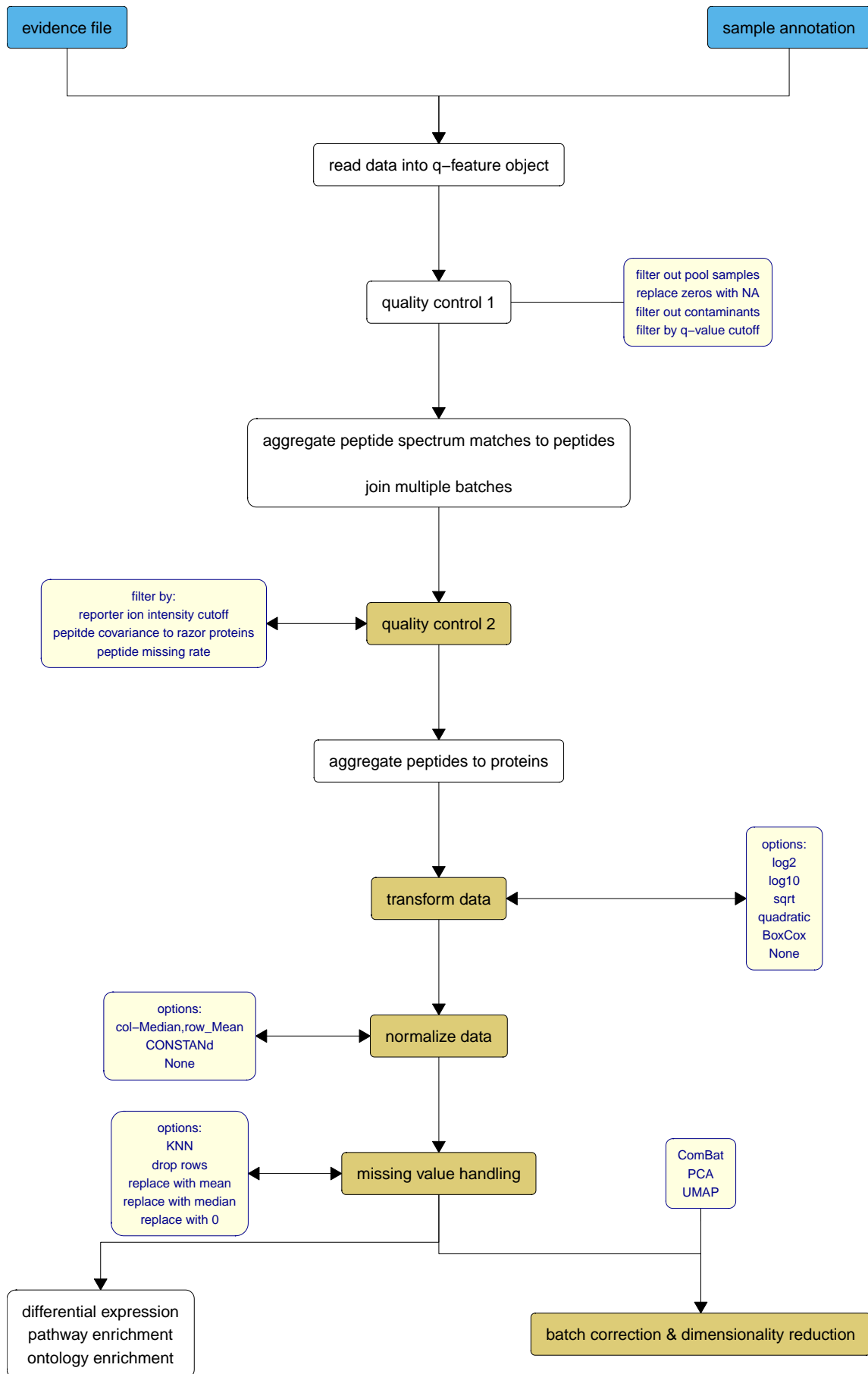


Figure 1: Flowchart presenting the processing by ProteoScanR

2.2.3 Processing the data

Further analysis is done with R and respective bioconductor packages. Please find version info in the appendix.

After processing MaxQuant creates a directory containing all results as .txt file. The evidence.txt file includes all peptide to spectrum matches (PSM) with their respective proteins and statistical parameters.

Example fo basic parameters and derivations include:

- Peptide sequence
- Mass to charge ratio (m/z) for all scans (eg. MS1, MS2)
- Retention time
- Precursor Ion Fragment
- Fraction of total spectrum
- Base peak fraction
- Reporter intensity (RI)
- Posterior error probability (PEP)

2.2.4 Object oriented programming

In order to streamline the analysis of multiple experiments, object oriented programming was applied. The approach in R is to create a so called Q-feature object, which contains all variables and metadata in a hierarchical structure. The structure enables sub setting for further analysis (Vanderaa & Gatto 2021).

2.2.5 Zero values

Peptides with low abundance are often set to zero during analysis. However, assigning a value of zero may incorrectly suggest that the sample does not contain the respective peptide. Given that it is highly unlikely for a biological cell of a comparable type and function to not contain a particular protein, replacing the zero value with “not applicable” (NA) is crucial for understanding and interpreting MS data. NA values will be managed in missing value handling later on the protein level.

2.2.6 Exclude reverse matches/contaminants

Peptide sequences matching to the reverse protein sequences (=decoy database) are considered as possible contaminants. These matches will be excluded from further analysis.

2.2.7 Filter according to precursor ion fraction (PIF)

During mass spectrometry, the ions detected in MS1 are further fragmented through collision during multiple MS runs. The resulting product ions are derived from precursor ions (also known as mother ions or parental ions). Contaminant peptides can co-migrate in this process and were distinguished by the lower fraction of their respective precursor ions (Tannous et al. 2020). These peptides need to be filtered out during the analysis pipeline. A cutoff value, referenced in the SCoPE2 pipeline (Specht et al. 2021), is applied in the user interface, but it can be adjusted.

2.2.8 Filter by q-value

The next step for quality control is the exclusion of samples with a high false discovery rate (FDR). When applying multiple statistical testing (e.g. t-Test) the obtained p-values can be considered as biased, because the probability to observe a significant will iteratively increase with each test performed. Corrections in statistics are an approach to compensate for the multiplicity of testing. There are many ways to do this compensation like the Bonferroni method or Benjamini-Hochberg's FDR. In Mass spectrometry the common "way to go" is calculating a false discovery rate, by dividing false PSMs (=hit of the decoy database) through the total number of PSMs above the peptide-spectrum matching score. The peptides spectrum matching score is defined as $-10 * \log(p)$. Whereas the p-value is defined that the hit is done by chance. The calculation of the score is highly dependent on the data acquisition method used. MaxQuant uses Andromeda, an integrated search engine. Proteome Discoverer from Thermo Fisher utilizes different engines such as Mascot or Minora. As published by J.Cox in 2011 Mascot and Andromeda showed similar performance when comparing FDR values as a function of coverage. However the observed performance can be lower when dealing with a decreased coverage (Cox et al. 2011).The threshold for accepting an FDR of an individual PSM is described as q-value.

2.2.9 Peptide spectrum match (PSM) aggregation to peptides

In data science, aggregation refers to a row-wise operation that merges data based on a particular column using a specific function. In the context of processing from PSMs to unique peptides, the desired column is the PSM sequence. To account for different distributions across multiple assays, the median of the channel is used as the function to aggregate multiple matches into one.

2.2.10 Join assays

Sample size is often a limiting factor in hypothesis testing. A strict quality control and the fact that TMT reagents are only available up to 18-plex can reduce the number of observed samples below the critical threshold, leading to an early end of analyses. To overcome this limitation, the provided software is capable of processing multiple runs simultaneously, allowing for testing of multiple batches and increasing the number of samples that can be included in the analysis. For further processing the runs are joined in one object at the peptide level.

2.2.11 Calculate median reporter ion intensity (RI) and filter

Columns which do not meet the desired intensity can be filtered by a threshold set on the RI. The median RI can also be used to check if an entire channel has a lower detection level. This can be due two reasons. One is the expression level of the given proteins in a cell. Meaning, that the expression of the observed cell type is simply lower than the other type. Another one could be a spillage of TMT detection in other channels due incorrect or missing correction of the TMT isotopes. The correction values can be found on the vendor's webpage (in this case Thermo Fisher) and correction needs to be set up in MaxQuant.

2.2.12 Calculate median coefficient of variation (CV) and filter

Depending having a bulk sample or single-cell sample choosing a minimum of observed peptides and a cutoff value for the CV, changes the level of confidence in the peptide data. The coefficient of variation of a peptide is considered as the ratio of the standard deviation to the mean and describes the relationship of the observed peptide signal over multiple proteins (=razor proteins). Peptides having a high coefficient of variation over many razor proteins are considered as noise and need to be filtered out before statistical analysis.

2.2.13 Remove peptides with high missing rate

Although missing value imputation can be performed during the analysis of multiple batches, peptides with missing detections across channels can be problematic for quantification. The proteomic composition of a biological sample is similar between replicates and even across groups. However, the threshold of missingness (described as a fraction of the row) can be set in the user interface and adjusted.

2.2.14 Aggregation of peptides to proteins

Similar to the already explained previous aggregation step the peptides will be further processed into their respective proteins after the quality control on the peptide level is performed. Finally an expression matrix for every protein and their respective channel column is returned. Each channel refers to a sample and contains the intensities of each protein found in the biological specimen.

2.2.15 Transformation of protein expression data

Data transformation applies a function to each value of a matrix or array, so that:

$$y_i = f(x_i)$$

Depending on the distribution of the values in the observed expression set, different transformations can be applied to fulfill assumptions for statistical testing. In the shiny application, various procedures are implemented and can be further expanded upon request from the user. The macrophage analysis done by Specht et al. mentioned in their SCoPE2 publication (Specht et al. 2021) uses the logarithm to the base 2 to spread a compacted distribution and remove skewness in the dataset. This transformation was used as a reference when comparing methods. However, using the logarithm to the base 10 may be an easy way to recalculate expression data in the mind and will also be facilitated by other transformation methods such as the boxcox method, which is also implemented in the application. When observing a wide distribution of small and large values of the expression set in a histogram, a square root transformation can help increase the variability of smaller values and decrease the variability of larger values. Depending on the distribution, the user has to decide which transformation to consider and verify that statistical assumptions are met after application with visualizations such as histograms, qq-plots, and MA-plots. For statistically inexperienced users, the boxcox transformation can help with this decision. Developed in 1964 by

Box and Cox (Sakia 1992), this method applies a linear model against 1 on the data to determine the statistical parameter lambda by the maximum likelihood method. The log-likelihood method takes the 95% confidence interval for the parameter lambda and the final lambda is chosen as the value with the highest log-likelihood value.

λ	Transformation
-2	$\frac{1}{x^2}$
-1	$\frac{1}{x}$
-0.5	$\frac{1}{\sqrt{x}}$
0	$\log x$
0.5	\sqrt{x}
1	x
2	x^2

Depending on the size of lambda, a certain function will be automatically applied to each value of the expression set in order to introduce normality. In terms of usability, the boxcox method is the most efficient transformation method, taking the decision of which calculation to apply away from the user.

2.2.16 Normalization

The term normalization is ambiguous in data-science and will be explained briefly in this chapter. Starting with converting the data to the Z-distribution (Gaussian result), where 0 represents the mean and 1 represents the standard deviation, in vectorization every feature (or protein) is represented as a vector that points in a specific direction in the unit sphere, normalization can have different meanings. Normalization is considered as part of the scaling procedure and ensures that every feature contributes equally to the statistical model and hinders large values from biasing the model in a particular direction. However, this could also have negative consequences for the modeling procedure, as it may reduce the impact of important features on the dataset. Depending on the algorithms later used in the data processing, the method of choice for normalization can change the results significantly. The K-nearest neighbor (K-NN) clustering algorithm, for instance relies on the distances between distinct data points by minimizing variance of the squared euclidean distances. This method will be applied in the missing value imputation, which will be the next step applied to the data. The first normalization method available in the user interface is column-wise median and row-wise mean normalization. This method was chosen by Specht et al in the SCoPE2 publication 2021 (Specht et al. 2021) and worked as a reference during the development process to benchmark

other methods. When dividing each value of an expression set by the median of the particular column, the procedure is considered as a column-wise median normalization. Although the mean-normalization works the same way but takes the mean as the second variable. In the analysis pipeline both procedures were applied on the dataset. However when the logarithm as the transformation method was chosen as transformation method, ProteoScanR automatically switches from a division to a subtraction, since: $\log_a \left(\frac{u}{v} \right) = \log_a u - \log_a v$. After applying this normalization method, each value can be interpreted as a distance or fraction of the mean or median of the corresponding column or row, enabling fair comparisons between features and samples. The second method for normalization included is the CONSTANd method, which was proven suitable for relative quantification in the field of proteomics (Maes et al. 2016, Houtven et al. 2021), but can also be applied on RNAseq data. CONSTANd uses a technique called matrix raking, which employs the RAS algorithm. The expression set reflects the non-negative real (m, n) matrix A where the bi proportional constrained matrix problem will be solved by finding the (m, n) matrix B which equals to $\text{diag}(x) * A * \text{diag}(y)$. Whereas $x \in \mathbb{R}^m$ and $y \in \mathbb{R}^n$. The solution to this problem involves finding the row sum of $B = u_i$ and the column sum of $B = v_j$, where i and j denote the row and column indices of the matrix, respectively (Bacharach 1965). In other words, the matrix will be alternatively manipulated on rows and columns until the mean of both equals 1. In order to apply the method and yield true results, one has to consider 3 major assumptions between sample types. This assumption can be observed in the MA-plot which indicates the differences of two samples. Given the intensities of two samples, R and G , visualized on a graph with the x-axis as $M = \log_2\left(\frac{R}{G}\right)$ and the y-axis as $A = \frac{1}{2} \log_2(RG)$. A comparison between all sample types of identically processed sets is needed before calculation and the assumptions must be fulfilled.

- **1 The majority of proteins are not differentially expressed**

Density of the dots decreases when looking from the middle of the cloud towards the edges.

- **2 Up- and downregulation is balanced around the mean expression**

The scatterplot of the data points is symmetrical around the mean on the horizontal axis.

- **3 Systematic bias correlates with the magnitude of expression**

The symmetry axis is approximately horizontal.

If the MA-plot does not visualize any of these violations the CONSTANd method can be applied on the dataset and the biological meaning of the sample types can be assessed. The method is utilized by the bioconductor package handler. Another method developed in the application is the quantile

normalization. Quantile normalization is performed over all columns, equalizing statistical parameters such as inter quartile range, median and mean. However the application of this method is only suitable if the number of differentially expressed proteins is approximately equal over sample types. Otherwise statistical power could be lost by removing fine deviations (Zhao et al. 2020). For the quantile normalization method the package limma was utilized. Quantile normalization ranks protein expression by magnitude, then averages the expression values occupying the same rank and substitute the initial value with the average. However if the dataset already consists of balanced features and samples or the user wants to benchmark the methods applied, normalization can be skipped also, by setting to “none”.

2.2.17 Missing value handling

When analyzing multiple batches simultaneously, it is possible to encounter situations where a particular protein is not detected in one of the batches. From a biological perspective, it is highly unlikely that a cell completely lacks a single protein, as it would imply a complete loss of function for that protein. Therefore, an intensity value of 0 is close to impossible for most proteins. In order to handle this dark space in the expression set, several methods can be chosen in the application. A variety of function employs replacing the missing values with the mean or median of the rest of the matrix. This procedure introduces no bias in the data if the missingness is low, although differential expression for the sample carrying the missing feature can not be expected as well. Even a more conservative approach is dropping the rows for the feature with the missing value in one of the observed samples. A common practice in proteomics is utilizing the K-nearest neighbor algorithm (=KNN), which imputes the missing values by a euclidean metrics of the neighboring values in the columns where the feature is not missing. K denotes for the count of neighboring values of a gene and can be selected upon preference. The euclidean distance between two points is defined as $d = \sqrt{a^2 * b^2}$, the K nearest neighbors average value will be assigned to the intensity of the missing feature. Since the average is a statistical metric which can be biased easily by skewed distributions, normalization is an important task before performing missing value imputation. KNN was benchmarked for the regression of protein abundance intensities and showed an Area under the Curve (AUC) above 0.7 when testing on a human proteome test set (Lan et al. 2013).

2.2.18 Batch correction

Since mass spectrometry experiments are highly influenced by several factors, such as sample processing, the technician, manufacturer and production of the device, the reagents etc., working in multiple batches introduces further variance in the protein data. This variance would overshadow the biological differences across sample types when performing dimensionality reduction. A common misconception in biology is, that batches need to be corrected before differential expression analysis, which is the final aim of ProteoScanR. It appears convenient to remove the batch effect before performing any statistical analysis, which is in turn prone to errors especially if the sample groups are not split equally between batches. In this case, group differences influence the batch effect reducing statistical power after the correction. These both effects are so called interdependent. The opposite could happen if the experimental design is heavily unbalanced leading to group differences induced by batch correction. Finally it is recommended to include the batch factor should in the linear model as a co-factor and statistically quantify it (Nygaard et al. 2016). However it could be of interest to observe biological relevance of the factor of interest in the dimensionality reduction visualization, so a batch correction option was included to meet this need. To address the non-biological experimental variations, also known as technical factors, the R package sva (Leek et al. 2012) with the ComBat function (Johnson et al. 2007) was used. The expression of a gene g for the batch m_i and sample j can be defined as $Y_{ijg} = a_g + X\beta_g + \gamma_{ig} + \delta_{ig}\epsilon_{ijg}$, where γ and $\delta\epsilon$ represent the systematic error caused by the batch. The Bayesian framework is employed to remove this systematic error by shrinking the effect and pooling information over the features g . Ideally the effects a and β remain as natural as they are and should reflect the true biological difference between experimental obtained samples or groups. Before applying batch correction, the data is standardized using Z-transformation. By the method of moments (= the mean and the variance) the two batch effect parameters γ and $\delta\epsilon$ were estimated and can be subtracted from each value for the particular feature driving statistical moments at a comparable level between batches. The ComBat function allows the user to specify a desired effect, which represents the actual biological variance to be preserved while removing non-biological variance. This is achieved by constructing a design matrix, which is provided as prior information about the dataset within the Bayesian framework. However, in cases of poor experimental design, the factors contributing to unwanted and desired variation may be confounded. In the worst case, if only one sample type per run is observed, it becomes challenging for the program to distinguish between batch-induced variance and biological variance. In such cases, the user is advised to adjust the experimental layout for future experiments. The detection algorithm for confounding effects is facilitated by QR matrix decomposition. The matrix $A = QR$ is decomposed

into an orthogonal matrix Q and an upper triangular matrix R . By comparing the rank of matrix A with the number of biologically relevant factors, it is possible to determine the presence of confounding effects in the dataset. The rank is defined as the maximum number of linearly independent columns. The same approach is used in the limma package (Phipson et al. 2016) to identify non-solvable coefficients in experimental designs.

2.2.19 Dimensionality reduction

After cleaning the data and crystallizing from impurities such as noise and unwanted effects, the biological differences between sample types can be obtained. Proteomic data consists of multi dimensions (=features) which are overall hard to understand by a glance. An approach to observe the differences without a closer sight of exact effect on the proteinaceous ensemble, but still keep a high level of information can be dimensionality reduction. After the cleaning procedures any additional effect caused by technical or biological replication should be removed, however it could be found be highlighting according to the particular factor. This makes the dimensionality reduction a useful tool before starting any statistical analysis by checking for involuntarily introduced bias.

2.2.19.1 Principle component analysis (PCA) The most common approach in data science for any kind of high dimensional data is the PCA. For ProteoScanR the bioconductor package scater (McCarthy et al. 2017) was used. Every principle component can be understood as a vector pointing in a specific direction derived as the eigenvector from the covariance matrix of the expression set. The covariance matrix indicates for the co linearity between the variance of all elements compared. After calculating the covariance matrix the eigenvectors for the covariance matrix will be obtained by solving the quadratic equations to obtain the eigenvalues λ . Since $Av = \lambda v$ the eigenvector v can be obtained by solving the equation for each element of the vector. The eigenvectors v never changes its direction and explains the covariance within the dataset and so also the mathematical differences between the samples. The eigenvectors are sorted according to their eigenvalues in decreasing order and therefore decreasing explained variance. For graphical visualizations the principle components are plotted against each other. The first two components, which explain the majority of variance in the dataset highlight the difference between samples.

2.2.19.2 Uniform manifold approximation & projection (UMAP) UMAP (McInnes et al. 2018) is a dimensionality reduction technique that was developed in recent years and is based on Riemann geometry. It shares similarities to the t-distributed stochastic neighbor embedding (t-SNE)

in terms of graphical visualization. Riemann geometry is a mathematical framework that deals with three dimensional functions using volumes, areas and vectors, which are also concept of topological data analysis. Before performing UMAP, three assumptions need to be considered:

1. There exists a manifold on which the data would be uniformly distributed. → This assumption implies that the probability for each value in the biological dataset is the same.
2. The underlying manifold of interest is locally connected. → In other words, similar samples will have a similar proteinaceous ensemble.
3. Preserving the topological structure of this manifold is the primary goal. → This means that the homeomorphic structure (the property of being able to transform one shape into another without tearing or gluing) is locally preserved, and local values in the dataset can be compared with each other.

(McInnes et al. 2018)

The UMAP algorithm begins by constructing a graph with a defined neighborhood parameter, typically denoted as k , which can be selected computationally. UMAP employs the k-nearest neighbor descent algorithm (NN-descent). Similar to the k-nearest neighbor algorithm (KNN), used in the missing value imputation part of this project, NN-descent recursively iterates to find the smallest distance to the respective neighbors within the defined neighborhood size k . Increasing the value of k gradually strengthens the clustering of the data, but at a certain point, fine structure may be lost, and only rough estimates of the underlying principle can be observed. The mathematical graph in UMAP is defined by nodes connected by edges, with each node internally connected to at least one other node. Edges are distinguished from each other not only by their connection but also by their importance, which is often referred to as weight. Whereas the weight function is calculated as

$$w((x_i, x_{i_j})) = \exp\left(\frac{-\max(0, d(x_i, x_{i_j}) - \rho_i)}{\sigma_i}\right)$$

and determine the parameter ρ for the weight function that:

$$\rho_i = \min \left\{ d(x_i, x_{i_j}) \mid 1 \leq j \leq k, d(x_i, x_{i_j}) > 0 \right\}$$

Furthermore σ will be set to meet the following conditions:

$$\sum_{j=1}^k \exp\left(\frac{-\max(0, d(x_i, x_{i_j}) - \rho_i)}{\sigma_i}\right) = \log_2(k)$$

and acts as a normalization factor. The obtained graph \bar{G} is called the fuzzy simplicial set which is obtained by approximating the geodesic distance (= locally length-minimizing curve) of the data points, leading to a topological approximation. The second phase of the algorithm adjusts the layout of the weighted graph to a representative view, but preserves the characteristics and shows the underlying topological principle of the data. In order to obtain a visual representation of the graph, the algorithm applies repulsive forces:

$$\frac{2b}{(\epsilon + \|y_i - y_j\|_2^2)(1 + a\|y_i - y_j\|_2^{2b})}(1 - w((x_i, x_j)))(y_i - y_j)$$

among vertices and attractive forces

$$\frac{-2ab\|y_i - y_j\|_2^{2(b-1)}}{1 + \|y_i - y_j\|_2^2}w((x_i, x_j))(y_i - y_j)$$

along edges. Where a and b are denoted as hyperparameters. By iterating through possible conformations until converging towards a local minimum with decreasing repulsive and attractive forces, the UMAP reaches it's aim to reveal the underlying properties of the data. The application utilizes the bioconductor package scater for performing UMAP (McCarthy et al. 2017).

2.2.20 Validation of the methods applied to the dataset

For the validation of methods applied to the dataset, the mutual information calculation is used to assess the impact of computations and the information it carries. Mutual information, denoted as $I(X; Y)$, is a measure of the dependence or information shared between two variables, X and Y , in this case sample types. It is calculated using the equation $I(X; Y) = H(X, Y) - H(X|Y) - H(Y|X)$, where H represents the entropy, $H(X|Y)$ and $H(Y|X)$ denote for the both conditional probabilities and $H(X, Y)$ for the joint entropy. Entropy, as a concept in information theory, quantifies the level of disorder or uncertainty associated with a random event. Events that are highly likely to occur are considered less informative than events that are more unexpected or less likely. In a Venn diagram $I(X; Y)$ (the mutual information) corresponds to the intersection of the two conditional entropies $H(X|Y)$ and $H(Y|X)$. To calculate the mutual information between two variables X and Y the above equation can be alternatively expressed as $I(X; Y) = D_{KL}(P_{(X,Y)}||P_X \otimes P_Y)$. D_{KL} denotes for

the Kullback-Leibler (Kullback & Leibler 1951) divergence which is a concept of relative entropy between two variables and tells us how much 2 probability distributions differ from each other. $P_X \otimes P_Y$ represents the product of the marginals. The underlying principle of divergence is the integral asymmetry in Bayesian inference, which means that divergence does not satisfy the triangle inequality. Differences are not the same depending on the starting point. By comparing the mutual information before performing any calculations with the mutual information calculated after the computations, it is possible to assess whether the applied methods have significantly altered the dependence or information content. The goal is to choose a method which preserves the information contributed by each biological sample type to the experiment. The R package “infotheo” is utilized to perform the estimates for the entropy of the two variables. Mutual information is returned as natural unit of information (=nat), a measurement proportional to the to the Shannon entropy ($1\text{nat} = \frac{1}{\ln 2} \text{shannons}$). Before calculating the pairwise mutual information of the expression matrix, values were discretized into bins with the discretize function of above package. The mutual information is calculated within each sample type, and it can also be calculated between a selection of sample types to determine if the computations performed affect the information content. After that all pairwise mutual information within the expression set before and after ProteoScanR is obtained. The pairwise differences can be observed as a boxplot for a particular sample type indicating the change in dependence within and also compared to another sample type.

2.2.21 Statistics

2.2.21.1 Differential expression After visualizing the biological tendency in the dataset, the next step is hypothesis testing. Several experimental designs can be tested against the null hypothesis h_0 , which states that there is no significant difference between the sample types. Before proceeding with any statistical testing, it is important to observe the data using either a quantile-quantile plot (qq-plot) or a histogram. The qq-plot serves a vital role in exploratory statistics by visualizing whether two datasets follow the same underlying distributions. In the case of statistical preparation for parametric tests, the first distribution is the dataset of interest, while the second dataset is the normal distribution. If the dataset follows an exact normal distribution, the values will align with the red line in the chart. However, values at the ends of the distribution may deviate from the normality line, indicating differentially expressed genes. These genes can be observed both in the histogram and the qq-plot. Parametric statistical tests rely on the assumption of normality in the data, which needs to be achieved before building a model. To achieve normality, it is recommended to try various combinations of transformation and normalization methods. By

observing the results in the plots, one can determine which combination of data processing methods satisfies the conditions required for the tests. However the limma method utilized in the statistics module shows great robustness to imperfect normal distributed values (Ritchie et al. 2015).

To test for differential expression, the analysis utilizes the “limma” package from R Bioconductor (Phipson et al. 2016). This package employs a linear model approach to determine the fold expression between sample groups. Before initiating the analysis, two matrices need to be computed. The design matrix identifies samples based on their sample type and defines the experimental design. An algorithm within the program’s backend logic is utilized to automatically generate this matrix according to the user’s selection in the interface. The expression matrix contains intensities for each identified protein and is obtained at the end of ProteoScanR. By calling a function with the design and expression matrices as arguments, the contrast matrix is calculated, enabling the user to decide which comparisons to consider and also perform tests on multiple factors. When observing multiple batches at once, as already explained in the chapter batch correction this effect needs to be taken into consideration when performing differential expression analysis. This is done by the multi-factor option in the user interface by selecting the batch as a co-factor and inclusion in the design matrix. The advantage of this procedure is, that the biological relevance of working in multiple batches can be quantified and the publishing of false positive results avoided. The multi factor option uses an additive model as a design matrix, whereas continuous variables (such as size, weight etc.) can also be used to build the statistical model.

The subsequent step involves creating a linear model between groups using log-ratios of their expression values. In a two-way design, the expression of the gene y can be explained as

$ExpY = \beta_0 + \beta_1 X_1 + \epsilon$, where β_0 represents the intercept, which can be interpreted as the mean expression of the gene. β_1 represents difference in mean of the treatment (or condition) on the discrete or continuous variable X_1 , and ϵ acts as an error term. The interface allows for additive models with multiple factors, allowing the user to add factors according to various scenarios. For example, in a two-factor model, it would look like: $ExpY = \beta_0 + \beta_1 X_1 + \beta_2 X_2 + \epsilon$. The principle remains the same for models with multiple factors. When visualizing the linear model, the x-axis would represent the gene for the sample types or other factors, whereas the y-axis would account for the expression value. By drawing a line through the cloud of data points the model is constructed by minimizing the quadratic distance to every data-point, called the least-square method or also ordinary least-square method. With the regression line the above mentioned equation can be constructed.

Next the statistical module of the program performs an empirical Bayes model utilizing the eBayes (Smyth 2004) function of the Limma package. The eBayes function utilizes a moderated t-statistics

following t-distributed values. The advantage of this method over the posterior odds is the reduction of hyperparameters to estimate used for the modelling process, also called shrinkage. In this context, the hyperparameters to estimate are the coefficient β_{gj} for gene g and sample i , as well as the variance σ_g^2 across genes g . In the Bayesian approach, probabilities are updated after obtaining new data, referred to as conditional probabilities. For estimation, it is assumed that $\frac{1}{\sigma_g^2} \sim \frac{1}{d_0 s_0^2} \chi_{d_0}^2$, representing the prior information of the model. The probability for $\beta_{gj} \neq 0$ is denoted as p_j , where p_j represents the expected proportion of truly differentially expressed genes. The expected distribution of log-fold changes follows the distribution $\beta_{gj} | \sigma_g^2, \beta_{gj} \neq 0 \sim N(0, v_{0j} \sigma_g^2)$. The posterior mean of σ_g^2 given s_g^2 is calculated as $s_g^{-2} = E(\sigma_g^2 | s_g^2) = \frac{d_0 s_0^2 + d_g s_g^2}{d_0 + d_g}$. This is where the shrinkage occurs, as the posteriors affect the prior values based on their respective sizes and degrees of freedom. The moderated t-statistic is defined as $\tilde{t}_{gj} = \frac{\hat{\beta}_{gj}}{\hat{s}_g \sqrt{v_{gj}}}$. Once the values of \tilde{t} and s^2 are calculated, the posterior odds are computed, providing the odds that a particular gene is differentially expressed. The odds for gene g being differentially expressed are denoted as $O_{gj} = \frac{p(\beta_{gj} \neq 0 | \tilde{t}_{gj}, s^2)}{p(\beta_{gj} = 0 | \tilde{t}_{gj}, s^2)}$, where the numerator represents the probability that the gene is differentially expressed, and the denominator represents the probability that the gene is not differentially expressed (Smyth 2004).

Limma outputs a table with all proteins, their respective logfold change, p-values and adjusted p-values. The user can choose different methods for the correction of the p-values, which is necessary when testing the same hypothesis multiple times. A common method in omics studies is the false discovery rate (=fdr) by Benjamini Hochberg (Benjamini & Hochberg 1995). By ranking all the p-values from smallest to largest the p-values are adjusted sequentially using the formula $p(i) = \frac{r_i}{m} Q$. The rank in the p-value table is denoted as r_i , m reflects the total number of tests and Q represents false discovery rate which is set to 5%. The second option to choose is the Benjamini & Yekutieli (=BY) (Benjamini & Yekutieli 2001)method, which is a further development of the fdr by the same statistician and has a wider range of application based on the dependencies for the test. The third and most conservative option is the Holm method (Holm 1979) which controls the error sequentially in a family wise manner, which is considered as traditional in regards to the above mentioned experimental wise error rates. The above mentioned correction methods are ordered in the way from the most liberal to the most conservative one. The selection is supposed to give the user the possibility questioning results on multiple levels.

2.2.22 Protein set enrichment analysis

After differential expression the upcoming question could be, in which context the up or down regulated proteins are. Enriched pathways can be understood as an over-representation (ORA =

over-representation analysis) of proteins within a specific set. This set, also known as ontology can be a pathway or a selection of common denominators in biological contexts, such as cell types or oncological factors. The statistical testing to identify the overabundant proteins of a specific set is similar to a χ^2 test developed by Karl Pearson (Pearson 1900) or the exact Fisher test (Sprent 2011) for tables with 4 fields in small sample sizes. Within the list are all truly differential expressed genes, an annotation is the identification of a protein in the desired biological context. The table is expected to be populated by the values as follows:

	in list	not in list	totals
with annotation	$(A+B)(A+C)/N$	$(A+B)(B+D)/N$	$A+B$
without annotation	$(C+D)(A+C)/N$	$(C+D)(B+D)/N$	$C+D$
	$A+C$	$B+D$	N

Under the null hypothesis H_0 states that the distribution and population of the table is random and there is no clear tendency with significant evidence. Against that the alternative hypothesis H_A says that there is an underlying tendency the table is populated. This leads to the test statistics, the observed values ($=O$) in the table are significantly different to the expected ($=E = \frac{(A+B \vee C+D)}{N}$) ones. One approach is approximating $\chi^2 = \sum_{i=1}^n \frac{(O_i - E_i)^2}{E_i}$ and deriving the p-value by the area under the density curve of the χ^2 distribution $Q = \sum_{i=1}^k Z_i^2$. In the distribution k is defined by the degrees of freedom ($=df$), what can be obtained by $k = (\text{columns} - 1) * (\text{rows} - 1) = df$ of the table. Another approach to obtain an exact p-value would be Fisher's exact test, which states that the margins are distributed according to the hypergeometric distributions. The test statistic leads directly to the p-value with no need for approximation: $p = 1 - \sum_{i=0}^{A-1} \frac{\binom{B}{i} \binom{D-B}{A+C-i}}{\binom{D}{A+C}}$. Here D denotes either for the background distribution which can be the total number of proteins obtained in the experiment, all proteins with annotation or a custom selected background. The background indicates all proteins which could be positive tested for in the observed sample. The above mentioned three options are implemented in the user interface. After obtaining the p-values for each protein set, the subsequent critical step involves the correction for multiple testing, considering the inherent risk of false positive results. Multiple testing correction methods adjust the significance thresholds to account for the increased probability of detecting false positives when performing multiple statistical tests. In this protein set enrichment analysis, the user is provided with a selection of established correction methods, akin to those commonly utilized in the field of differential expression analysis, ensuring robust and reliable interpretation of the results. Once the enriched protein pathways are determined, they can be visually represented using bar or dotplots, and a network of the found pathways.

2.2.22.1 Pathway enrichment analysis The pathway enrichment analysis is performed using the R Bioconductor package clusterProfiler (Wu et al. 2021). The analysis utilizes the entire “Kyoto Encyclopedia of Genes and Genomes” (KEGG) database, which is accessed through a function that maps the UniProt IDs to corresponding pathways.

2.2.22.2 Custom ontology based protein enrichment analysis For custom ontologies the protein enrichment analysis is done using the R bioconductor package piano (Väremo et al. 2013). In opposite to the pathway enrichment, piano maps proteins to a pre-selected gene collection set, which can be either downloaded from gsea-msigdb.org or custom made for the particular experiment and explains conditions, phenotype or other desired properties. The online database offers pre-built gene set collections for previous research questions in multiple fields of human biology. For statistical testing the above explained Fisher exact test is used. The output of the Fisher test does not show any directionality in regards of protein expression. If the user wants to include directionality in the network diagram, the default option of piano can be included in future versions of the program.

3 Results

To begin using the application, the first step is to upload the tab-delimited evidence file and the sample annotation file. Once these files are uploaded, the application is ready to run with default values. The default settings are preconfigured for an initial analysis, and any further adjustments or fine-tuning can be made in subsequent steps of the analysis process.

Proteomics Workbench

by Lukas Gamp

The screenshot shows the left panel of the Proteomics Workbench interface. It includes fields for uploading PSM and sample annotation files, setting input cutoffs for ion fraction and q-value, specifying minimal peptide observations, choosing protein transformation and normalization methods, and options for multiple batches. A 'Default' button is also present.

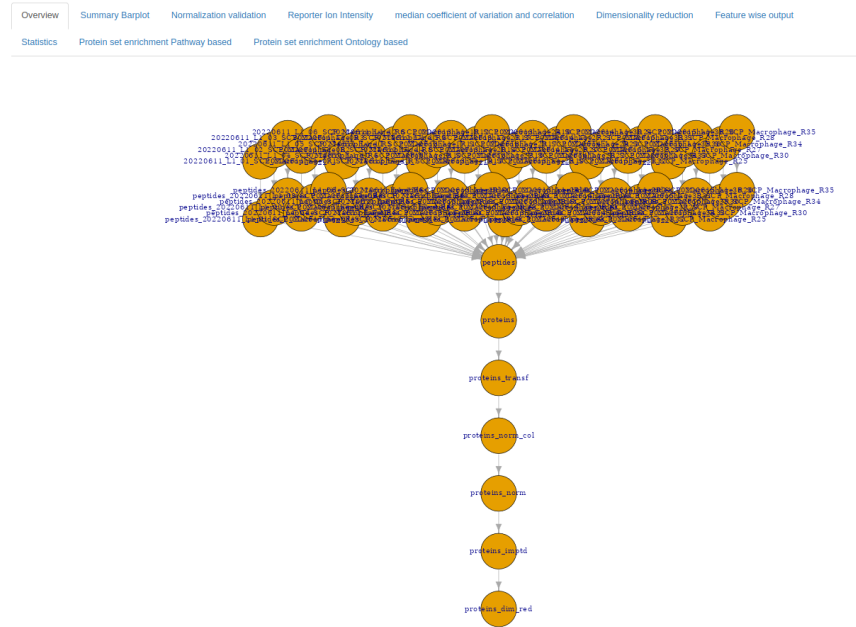


Figure 2: Summary showing the process of the analysis pipeline

After a runtime of 2 minutes on the 4 core laptop the data is ready to visualize. On the left side of the user interface, users can find the analysis pipeline settings that can be adjusted. Once the desired changes are made, they can be applied by clicking the update button. This allows users to observe the direct impact of the applied changes on the dataset. In the summary visualization, it may appear cluttered due to the processing of 36 files. In smaller datasets, the nodes of the network graph can be more easily distinguished and understood. When running the application with SCoPE2 (Specht et al. 2021) reference cutoffs, the following results were visualized.

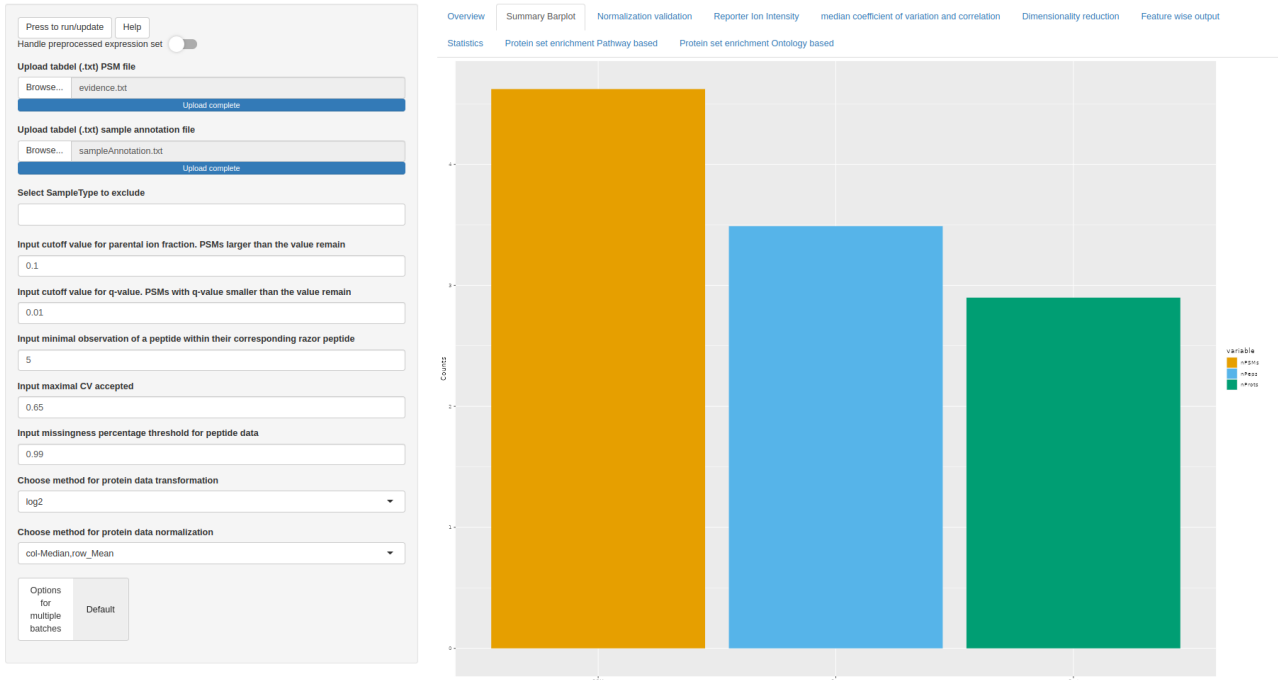


Figure 3: Barchart showing the number of peptide spectrum matches, peptides and proteins

The default settings of the analysis pipeline resulted in a total number of unique proteins below approximately 10^3 , which were aggregated from around $10^{3.5}$ peptides. Before these peptides were aggregated over approximately $10^{4.5}$ peptide spectrum matches. The aggregation method used is fixed by median.

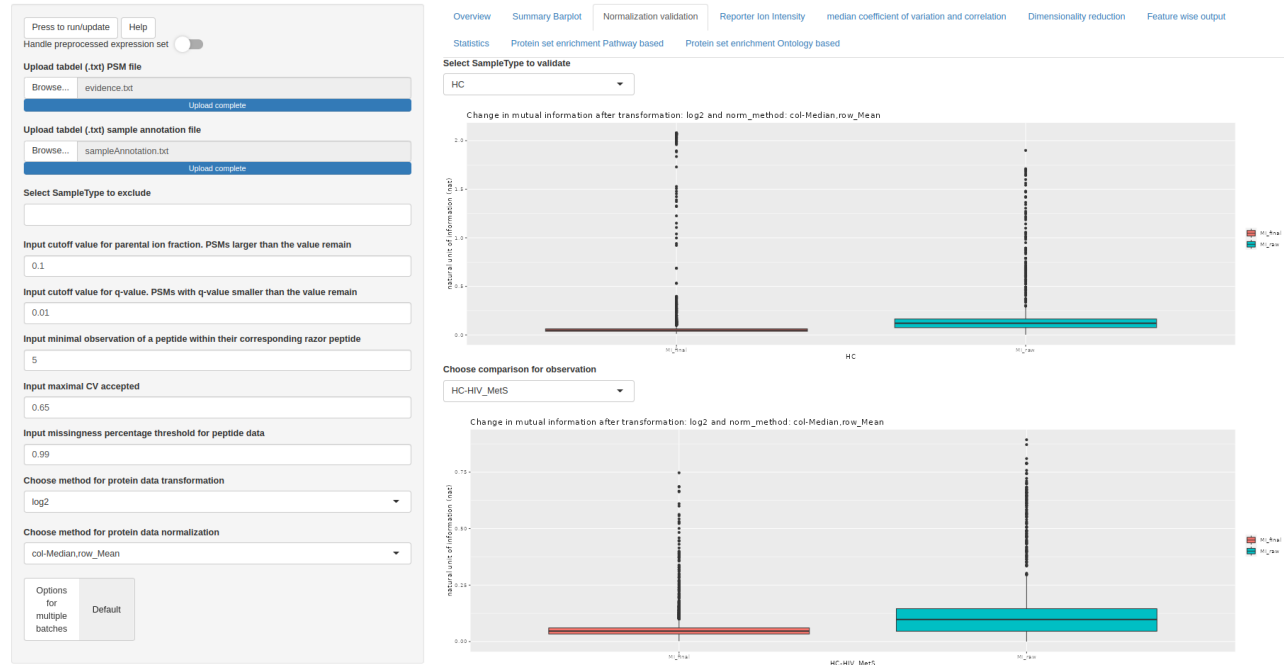


Figure 4: Mutual information with default setting

After applying logarithmic transformation to the base 2 and performing column median row mean normalization, the mutual information (MI) within the healthy control (HC) group's sample type exhibits a reduction towards the lower edge of the interquartile range (IQR).

MI between the HC group and the sample type corresponding to individuals with both HIV and metabolic syndrome, the IQR is further reduced and shifted towards the lower end compared to the MI values observed in the raw data.

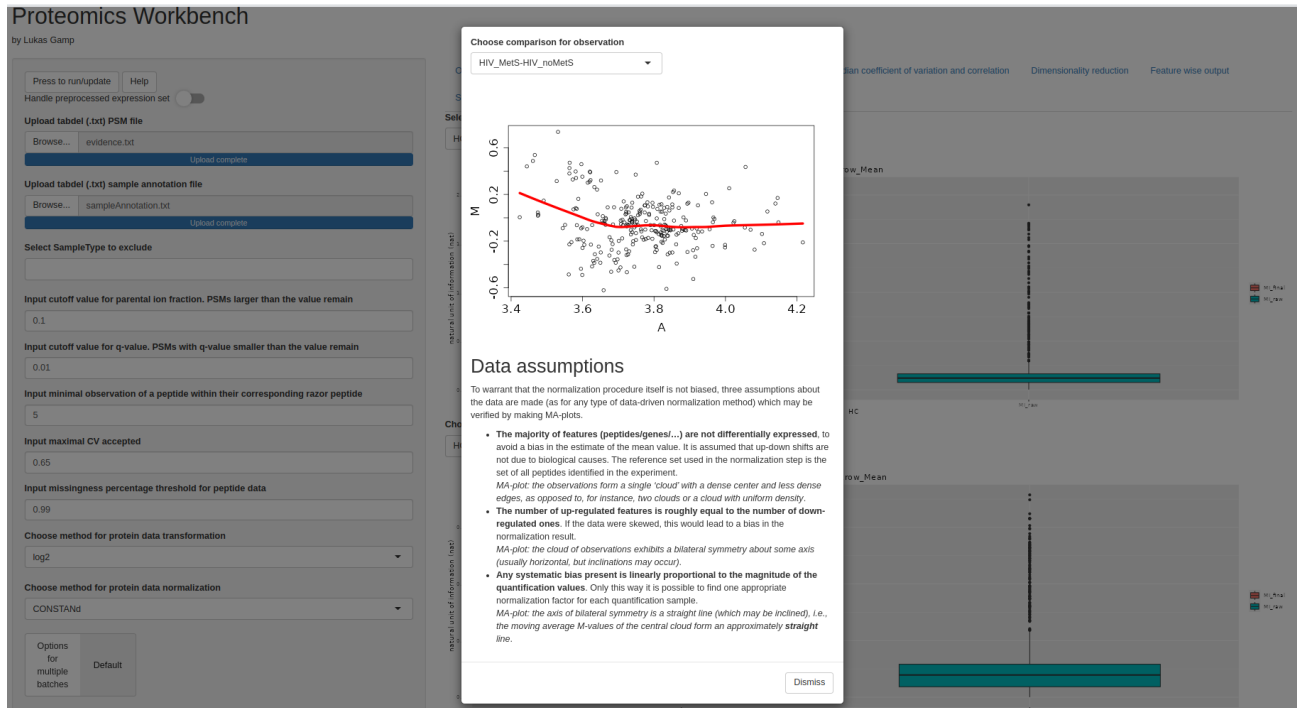


Figure 5: Popup showing the dependencies for the CONSTAND normalization

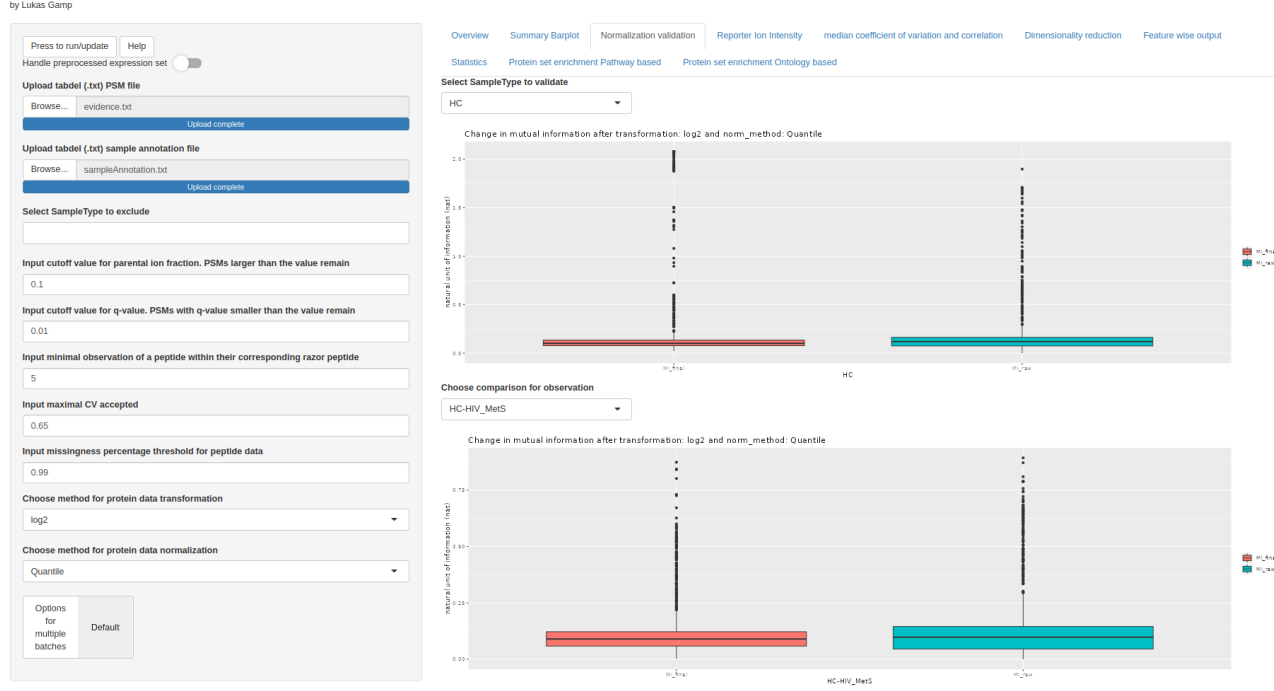


Figure 6: Mutual information with quantile normalization

After performing a logarithmic transformation to the base 2 and quantile normalization, the mutual information (MI) within the healthy control (HC) group's sample type exhibits a minor reduction in the interquartile range (IQR). However, it should be noted that there is an increase in the number of outliers compared to the raw data.

Observing MI IQR of the HC group with the sample type corresponding to individuals with both HIV and metabolic syndrome, the reduction in MI falls within the interquartile range of the raw data MI. Additionally, the median remains close to unaffected, indicating that the overall central tendency of the MI values is relatively preserved.

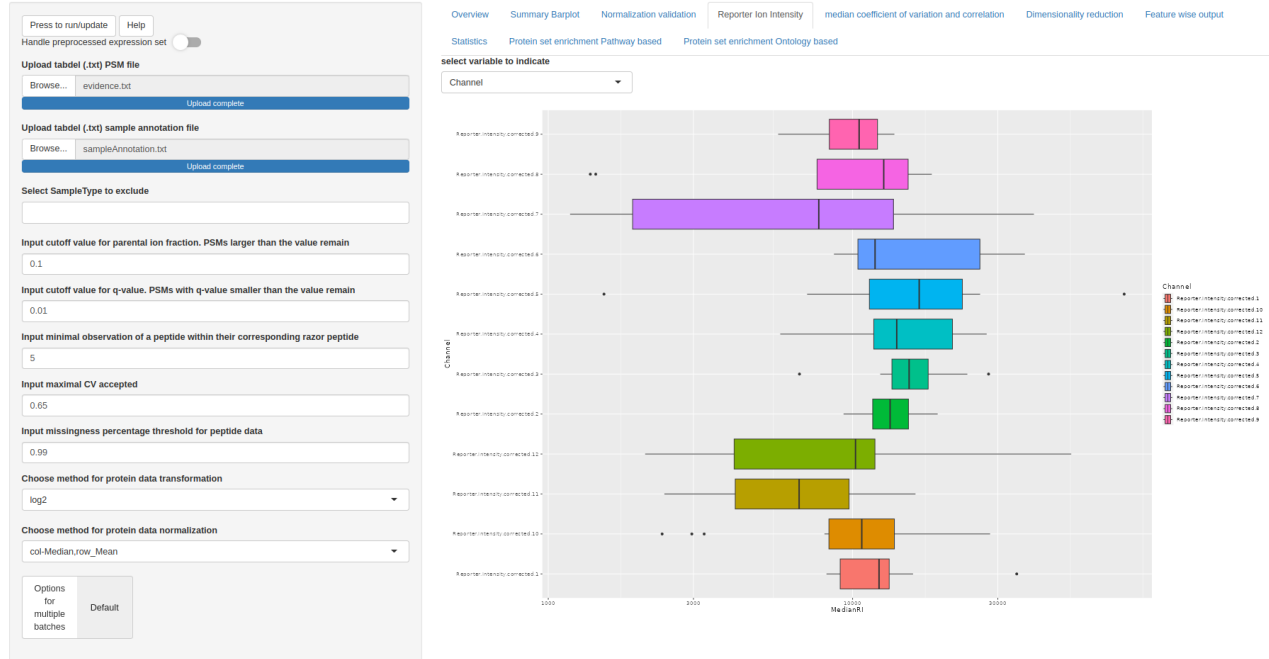


Figure 7: Reporter ion intensity with selection on channel. The selected factor will be highlighted and indicated in the legend.

When comparing the median reporter ion intensities across channels, no systematic bias is observed. However, it is worth noting that channel 7 exhibits a wide range of values spanning an order of magnitude. This comparison is crucial since the three sample types consistently occupy the same channels in every run, making the visualization an important aspect of the analysis. Despite the wide range of values in channel 7, there is still overlap in the interquartile ranges (IQR) across the majority of samples.

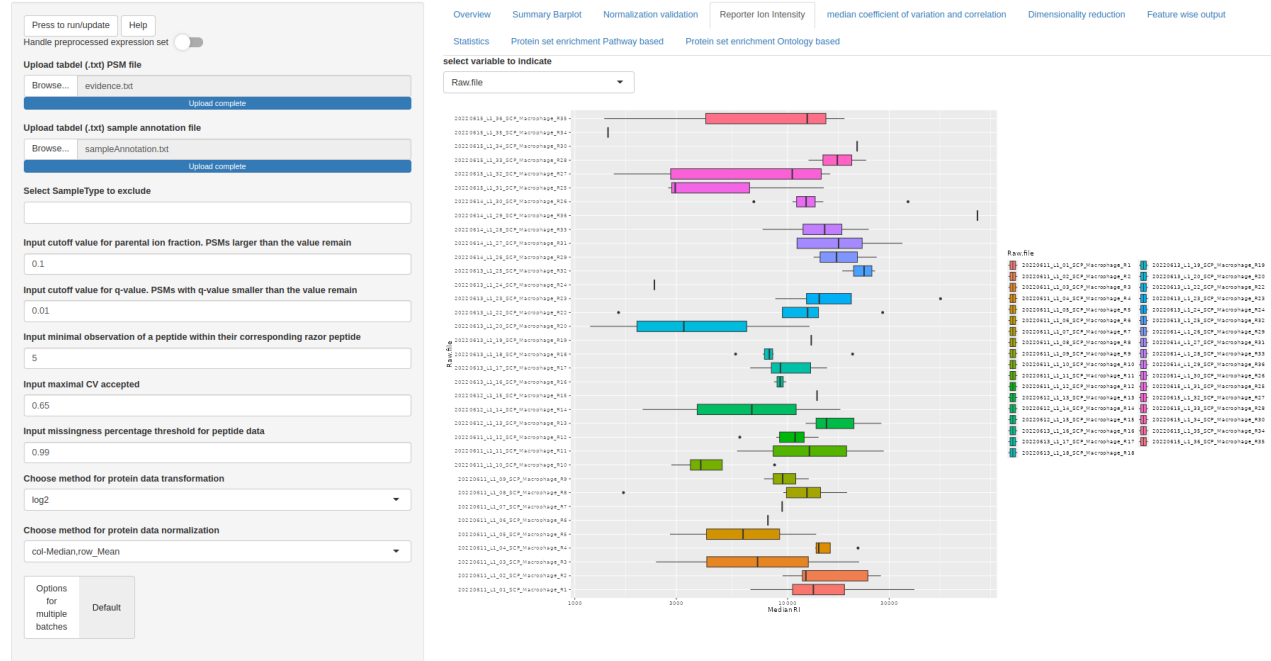


Figure 8: Reporter ion intensity with selection on file

Comparing the median reporter ion intensities with a focus on the batch (=Raw.file), it becomes evident that there are significant changes in signal that need to be taken into account in further analysis. After applying quality control measures, several values have been lost due to cutoffs in parameters such as parental ion fraction (PIF), q-value, coefficient of variation, and missingness of peptide data.

For dimensionality reduction, the user has the option to choose the batch correction method ComBat (Leek et al. 2012) in the side panel. However, this option is not set as the default choice. Instead, the conservative approach is followed, where the batch factor is included in the statistical module to account for any potential batch effects that may influence the results.

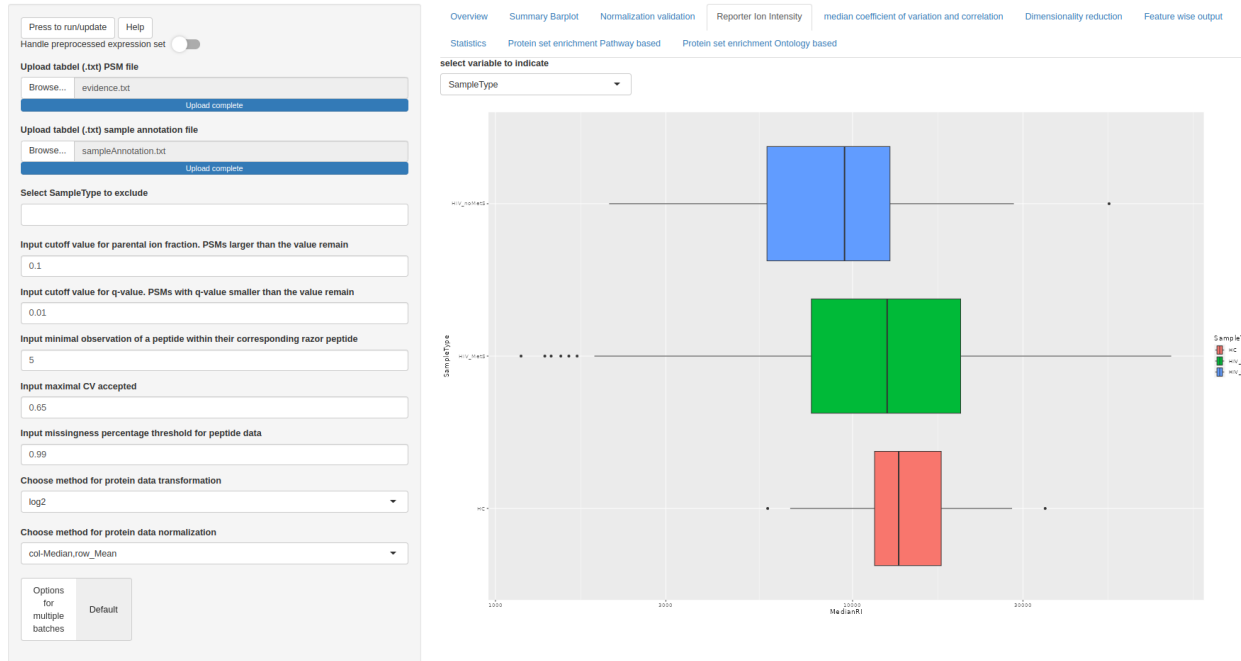


Figure 9: Reporter ion intensity with selection on sampletype

The sample type does not appear to have an impact on the median reporter ion intensities, as suggested by the overlapping interquartile ranges (IQRs). Nevertheless, the HIV group with metabolic syndrome displays a broader range of values spanning tenfold in arbitrary units.

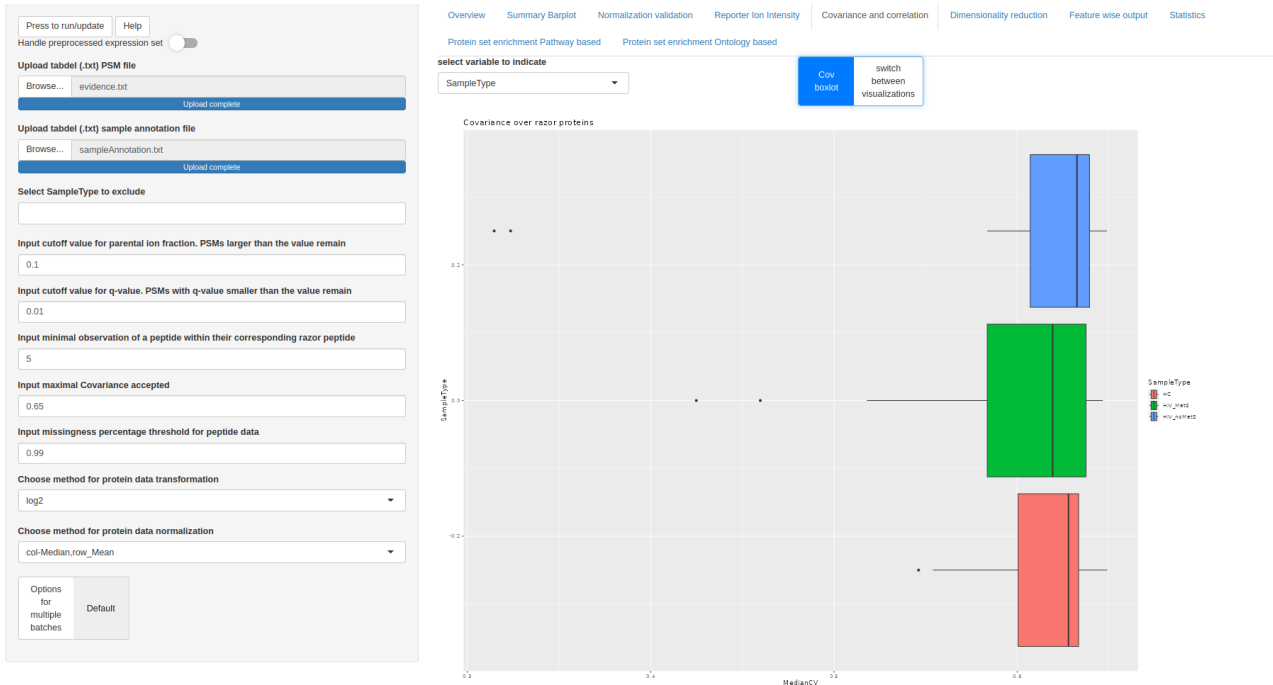


Figure 10: Median covariance of razor proteins with selection on samptype

A cutoff value of 0.65 for the coefficient of variation (CV) of razor proteins as shown in the SCoPE2 publication (Specht et al. 2021) demonstrates a satisfactory fit to the data. The minimum number of observations determines the threshold for considering a razor protein ambiguous, based on the number of matching peptides. In this case, the reference publication set the threshold at 5 observations.

The interquartile ranges (IQRs) remained unchanged by this cutoff. The sample type did not influence the CV of razor proteins. Boxplots illustrate that the values are distributed similarly, as indicated by the overlapping IQRs.

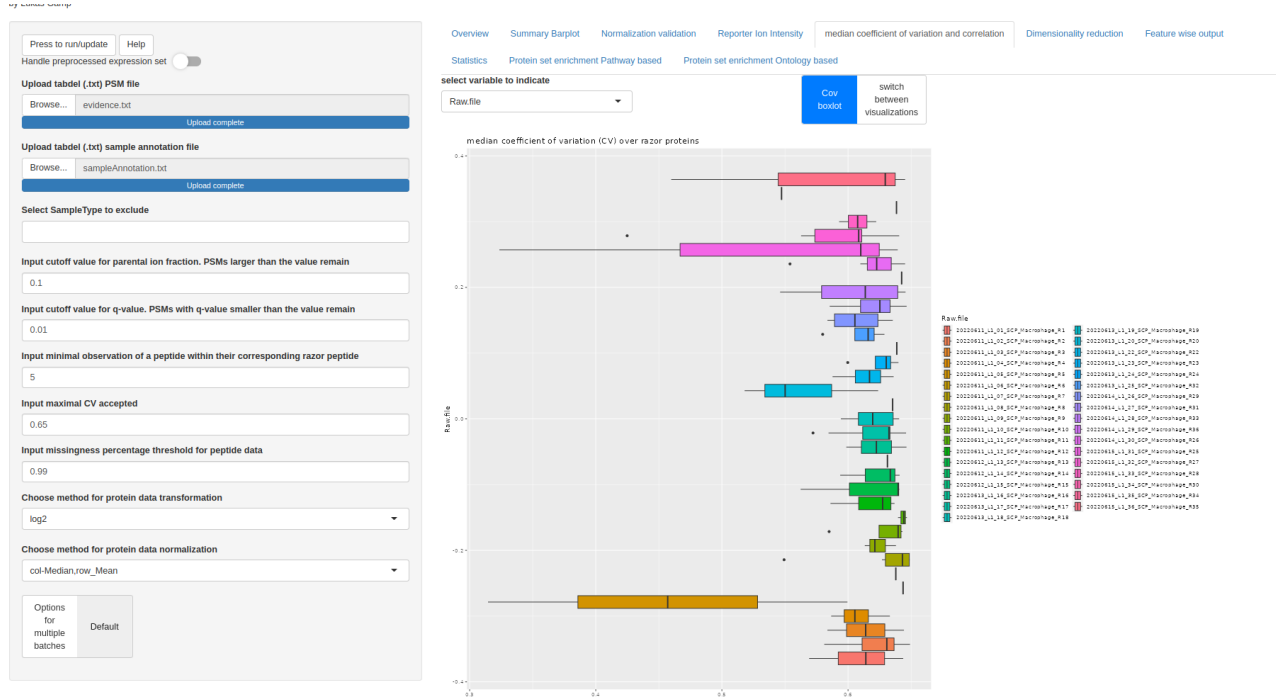


Figure 11: Median coefficient of variation (CV) of leading razor proteins per cell with selection on Raw.file

The plot illustrates that certain batches (=raw files) exhibit a higher number of distinct matches compared to others, as indicated by a thin line depicting low density. Most interquartile ranges (IQRs) overlap, suggesting similarity among the majority of batches. However, specific batches display a lower IQR in median CV across razor protein peptides, indicating distinct matches.



Figure 12: Median coefficient of variation (CV) of leading razor proteins calculated for 2 observations per cell, with selection on Raw.file

By setting the number of observations to 2, the distributions become more equalized. Additionally, batches that initially exhibited a decreased coefficient of variation (CV) tend to inflate towards the threshold.

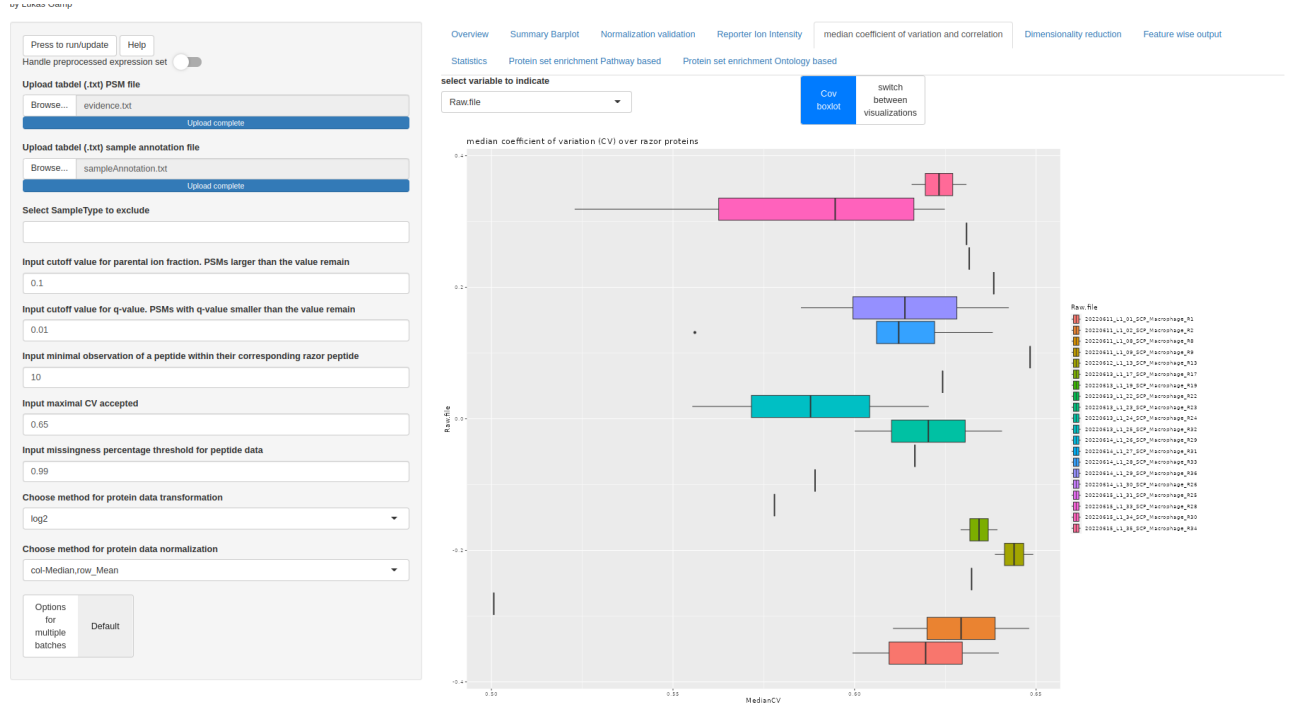


Figure 13: Median coefficient of variation (CV) of leading razor proteins calculated for 10 observations per cell, with selection on Raw.file

When the minimum number of observations for ambiguous peptides is set to 10, the distribution of medians across channels shows a decrease in density. This can be attributed to the rare occurrence of 10 unique peptides matching to the same protein, which is not commonly observed in the dataset.

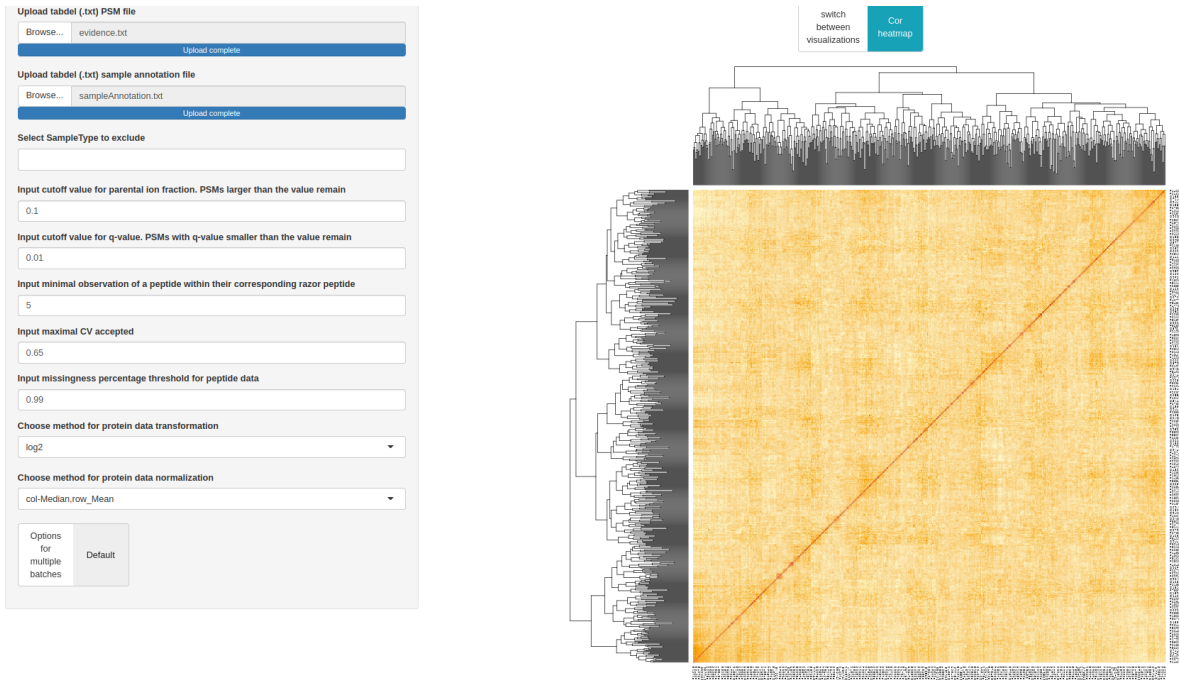


Figure 14: Correlation heatmap

The heatmap reveals the Pearson pairwise correlation coefficients between all proteins. The dendrogram indicates that there are two main protein clusters, with one of the clusters showing further sub-clustering, indicating a strong relationship among the proteins in the sub groups. However, the other cluster, consisting of individual proteins, shows weaker correlations, leading to a more intricate branching pattern in the dendrogram.

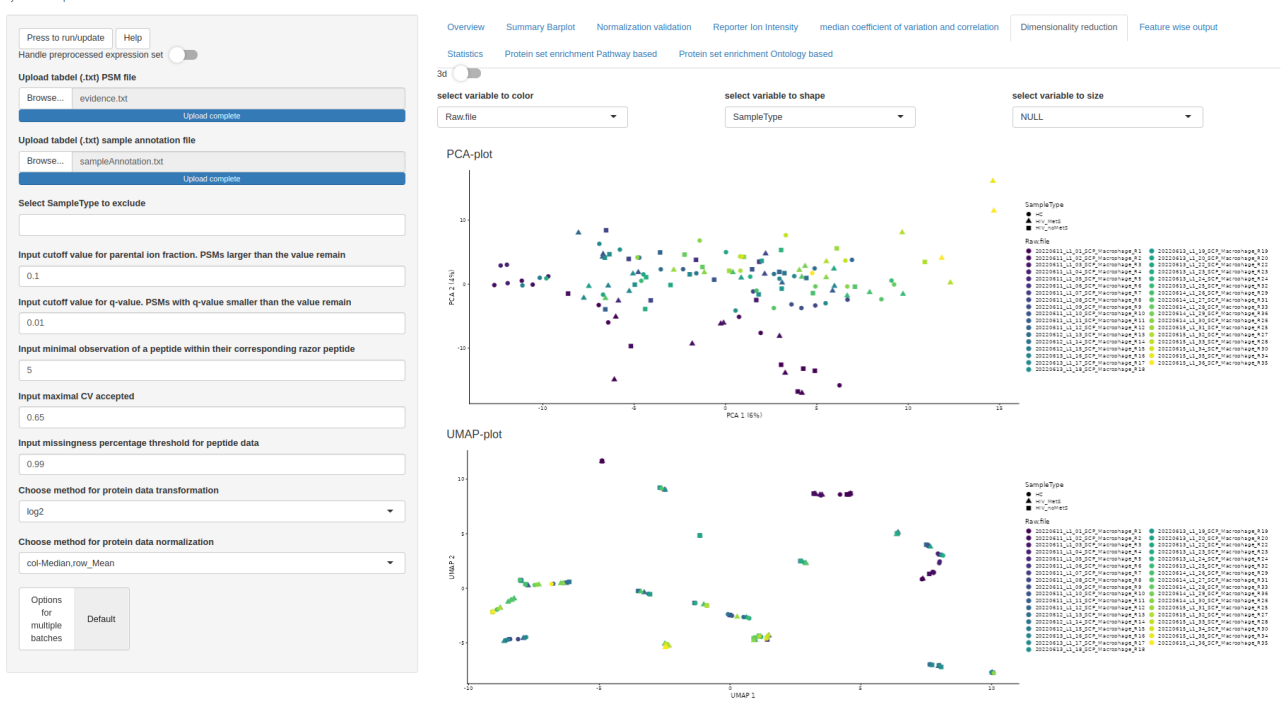


Figure 15: Dimensionality reduction analysis depicting sample types (indicated by shape) and raw files (indicated by color). Top: principle component analysis (PCA). Lower: Uniform Manifold Approximation and Projection (UMAP)

In both the Principal Component Analysis (PCA) plot and the Uniform Manifold Approximation and Projection (UMAP) plot, the second component is plotted against the first component.

Surprisingly, neither visualization reveals any discernible clustering patterns based on sample type or batch. For the k-nearest neighbor descent algorithm (NN-descent) employed in the UMAP, first a default value of $k=3$ was selected.

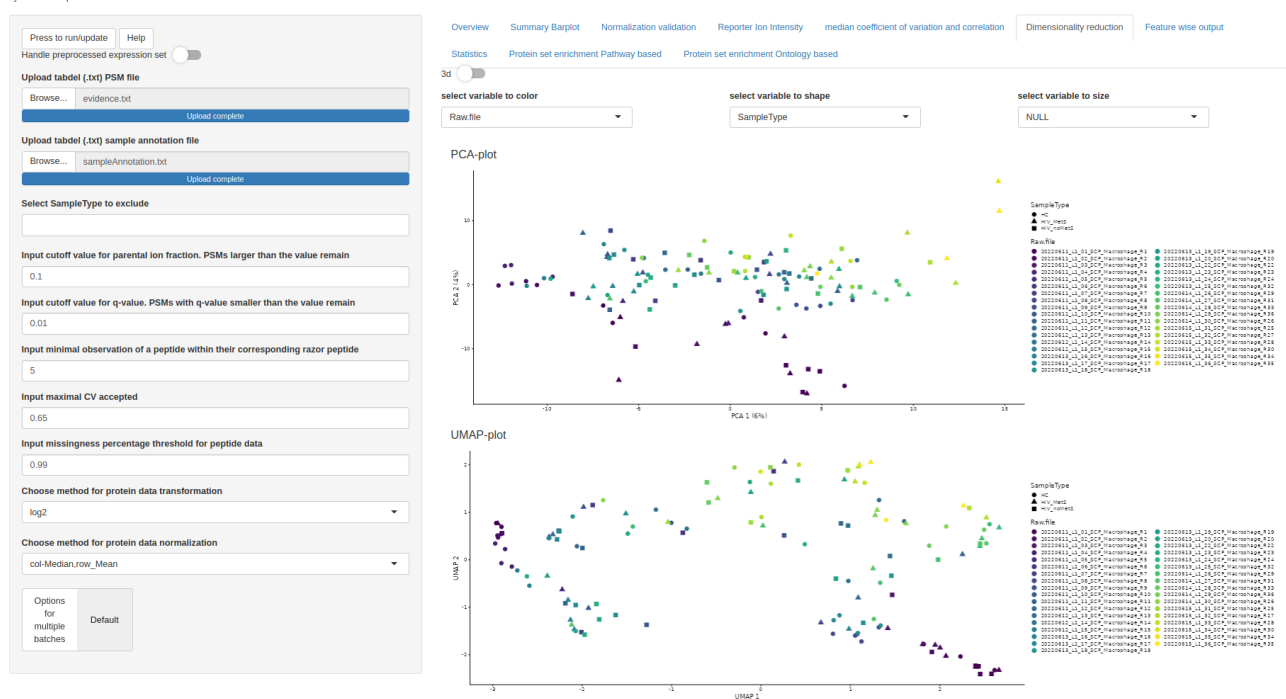


Figure 16: Dimensionality reduction analysis showcasing sample types (represented by shape) and raw files (represented by color). Top: Principal Component Analysis (PCA). Bottom: Uniform Manifold Approximation and Projection (UMAP). For the UMAP visualization, the k value for the NN-descent algorithm was modified to 15.

The second figure of the Principal Component Analysis (PCA) plot and the Uniform Manifold Approximation and Projection (UMAP), both displaying the second component against the first. Surprisingly, neither visualization reveals any discernible clustering patterns based on sample type or batch information. To enhance the resolution and capture more intricate patterns, the k-nearest neighbor descent algorithm (NN-descent) was adjusted, with a value of K set to 15. While the resulting plot exhibits improved detail, the underlying biological context or background remains elusive and does not emerge in the visual representation.

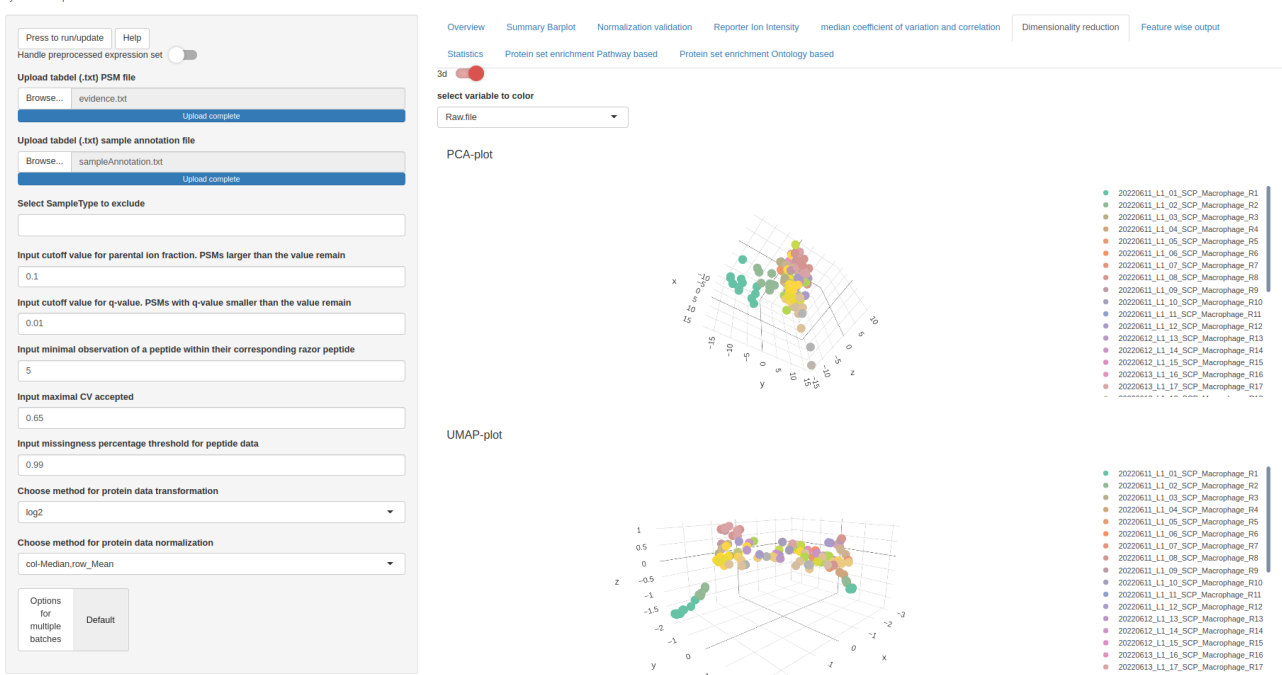


Figure 17: 3D visualization of dimensionality reduction analysis showcasing sample types (represented by shape) and raw files (represented by color). Top: Principal Component Analysis (PCA). Bottom: Uniform Manifold Approximation and Projection (UMAP)

In the 3D visualization, a subtle clustering pattern can be observed for the first two batches. Upon switching to the indicator sample type in the 3D visualization, no clustering can be observed whatsoever. This suggests that the variance in the data set is not attributed to sample type or batch, reinforcing the notion that other factors could contribute to the observed variability.

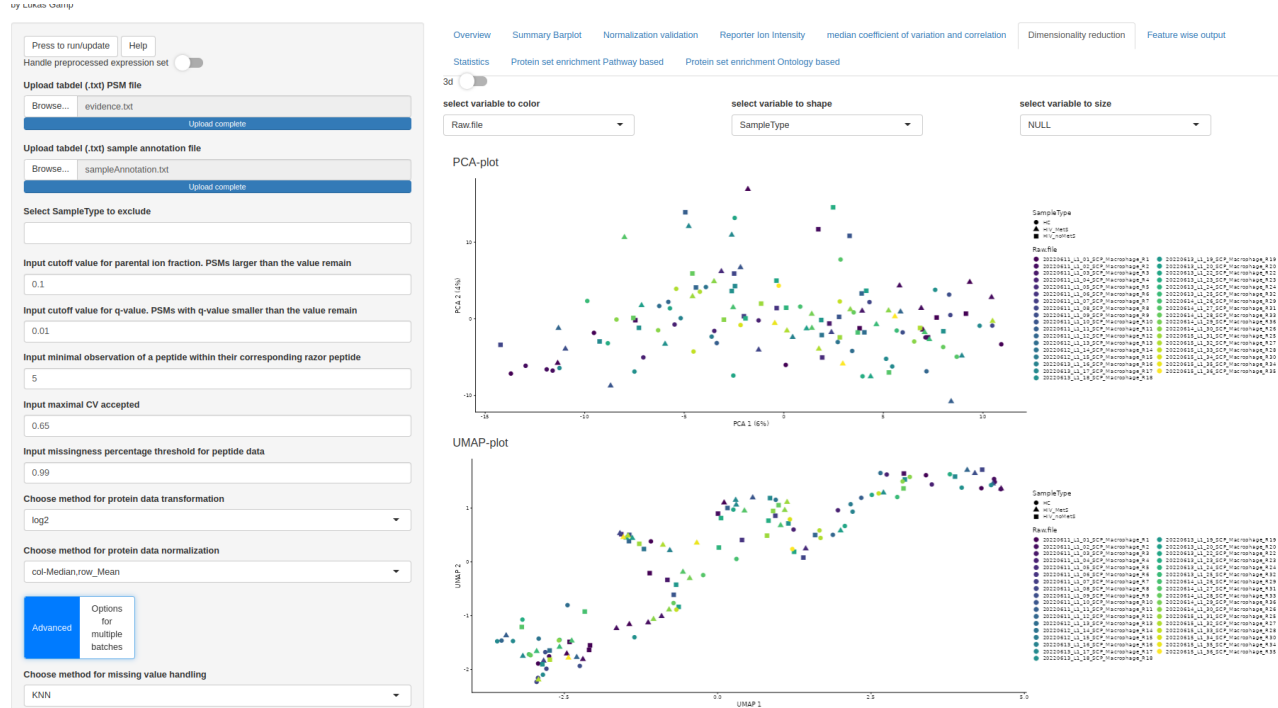


Figure 18: Batch corrected dimensionality reduction analysis showcasing sample types (represented by shape) and raw files (represented by color). upper top: Principal Component Analysis (PCA). upper bottom: Uniform Manifold Approximation and Projection (UMAP). lower top: 3D Principal Component Analysis (PCA). lower bottom: 3D Uniform Manifold Approximation and Projection (UMAP)

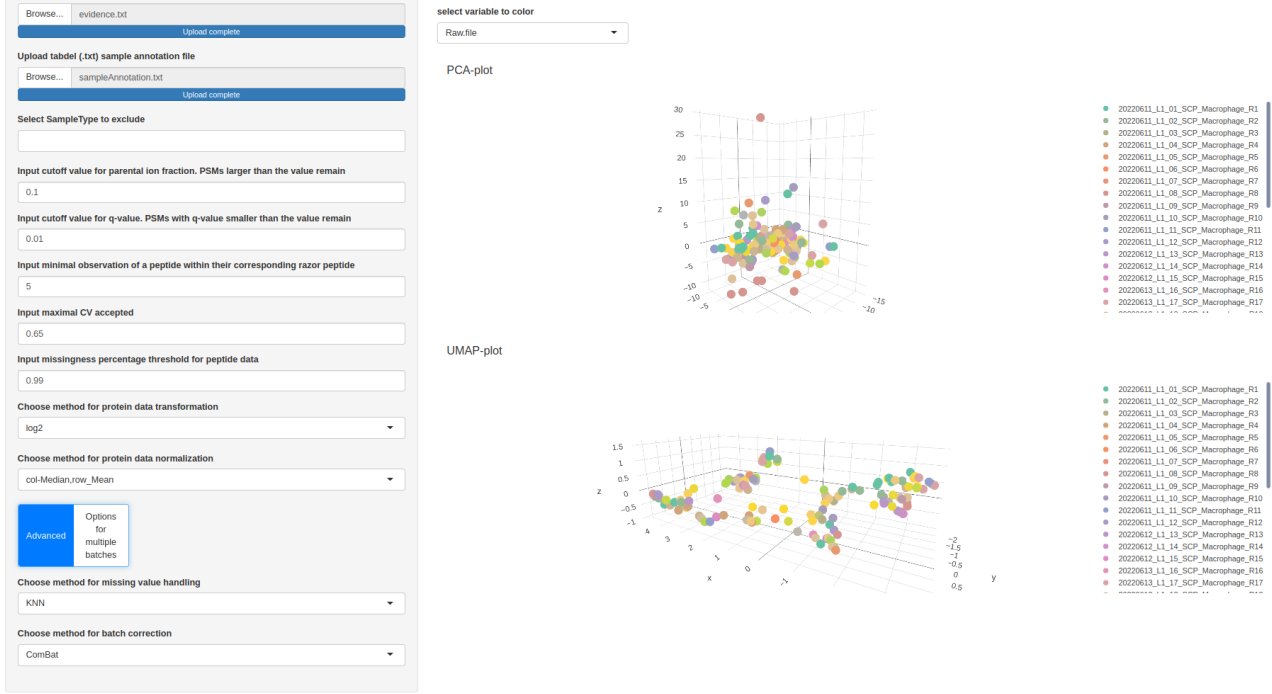


Figure 19: Batch corrected dimensionality reduction analysis showcasing sample types (represented by shape) and raw files (represented by color). upper top: Principal Component Analysis (PCA). upper bottom: Uniform Manifold Approximation and Projection (UMAP). lower top: 3D Principal Component Analysis (PCA). lower bottom: 3D Uniform Manifold Approximation and Projection (UMAP)

After applying batch correction using ComBat (Leek et al. 2012), neither the 2D nor the 3D visualization demonstrates any noticeable effects related to batches or sample types. The previously observed subtle clustering of the first two batches is now eliminated, indicating successful batch correction. However, it's important to note that the default pipeline was executed without batch correction for correct statistical testing.

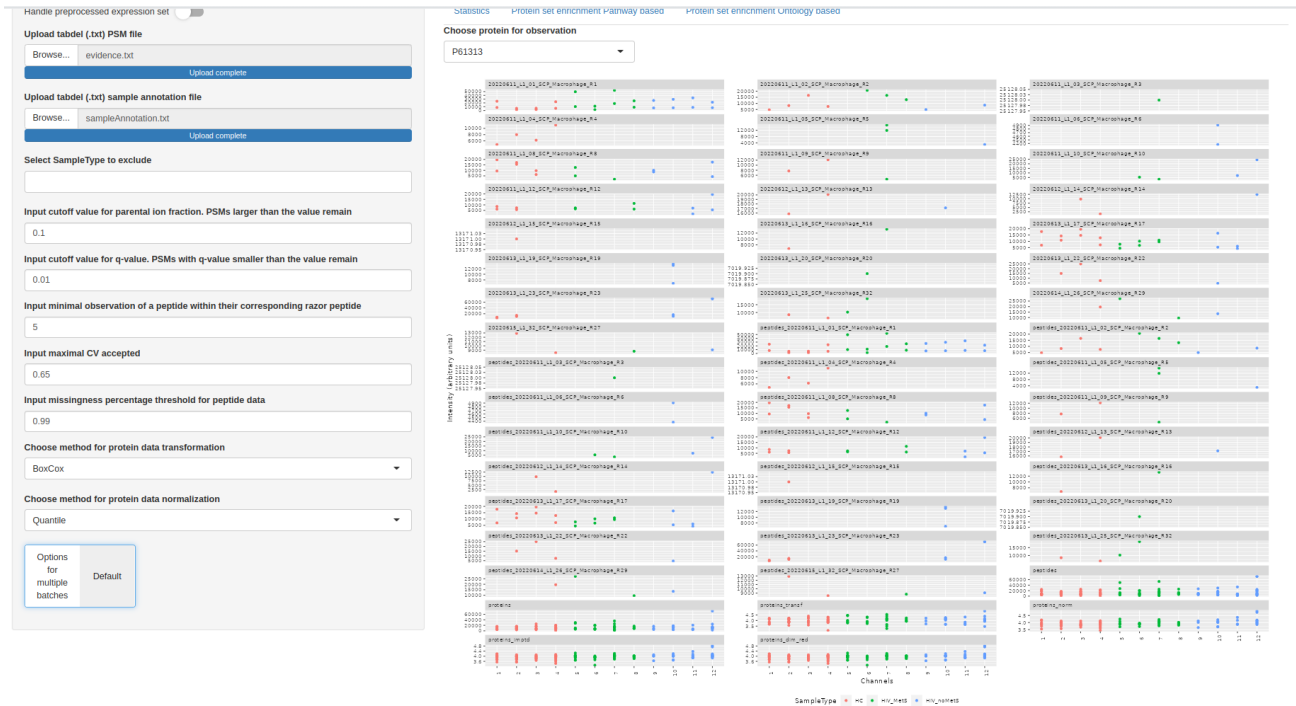


Figure 20: Feature wise output for the protein P61313 (=60S ribosomal protein L15) over the course of the pipeline.

The scatter plots indicate the detected values associated with the protein UniProt ID P61313 (= 60S ribosomal protein L15). Starting from the peptide spectrum level and progressing to peptides aggregated for individual raw files, these plots offer a comprehensive view of the protein's peptide abundance across various batches. As indicated 14 batches show no abundance of peptides derived from the protein P61313 at all. After merging the batches, the peptides appear to be abundant in all channels.

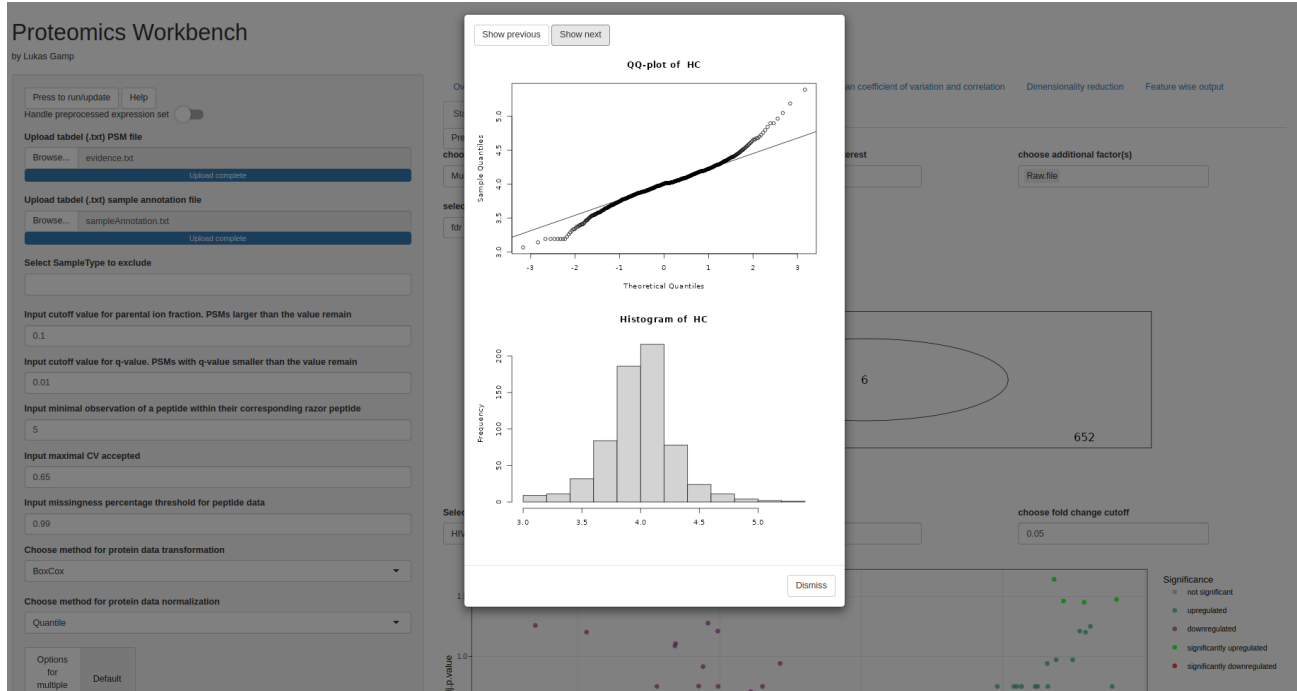


Figure 21: Popup window for checking the dependency of the statistic module

The t-statistics employed in limma are known for their robustness in handling non-normally distributed values. Nonetheless, it is recommended for users to assess the distribution of their data based on sample types before proceeding with statistical analysis. If the user is not satisfied with the results or identifies any distributional issues, the user can consider revisiting the transformation or normalization steps to address any concerns or improve the data distribution prior to statistical analysis.

The values for all sample types exhibit a unimodal distribution. However, when examining the quantile-quantile (qq) plot, heavy tails can be observed for all three groups. This indicates deviations from a perfectly normal distribution, suggesting potential outliers in the data.

Overview Summary Barplot Normalization validation Reporter Ion Intensity

median coefficient of variation and correlation Dimensionality reduction

Feature wise output Statistics Protein set enrichment Pathway based

Protein set enrichment Ontology based

Press to run statistics check dependencies for linear model

choose your study design choose your contrast of interest choose additional factor(s)

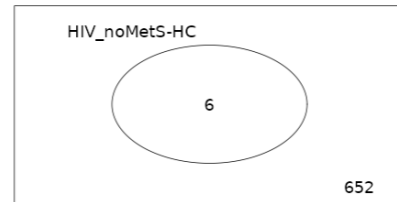
Multi factor additivity

HIV_noMetS HC

Raw.file

select method for p-value correction

fdr



Select your coefficient of interest

choose p-value cutoff

choose fold change cutoff

HIV_noMetS-HC

0.05

0.05

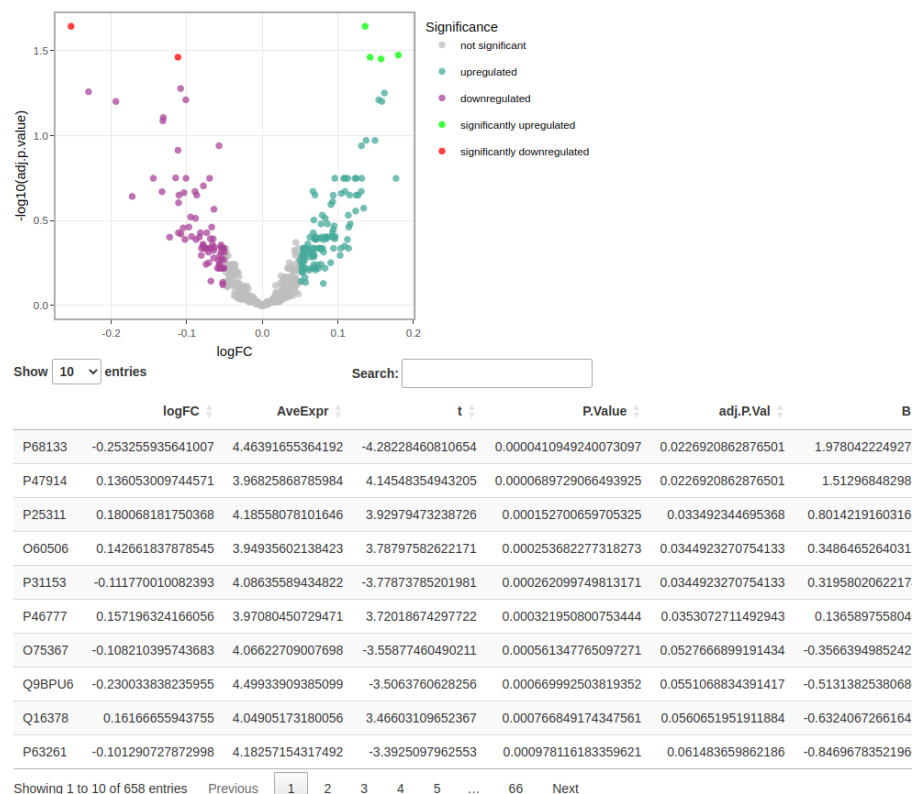


Figure 22: Statistic module

By comparing the log10-transformed and quantile-normalized expression values between the HIV group without metabolic syndrome and the healthy control (HC) group, six differentially expressed proteins were identified. The Venndiagram indicates significantly up/downregulated proteins. The Volcano represents -log10(adjusted p values) against log2 fold changes (logFC). These proteins include P68133 (Actin, alpha skeletal muscle), P47914 (60S ribosomal protein L29), P25311 (Zinc-alpha-2-glycoprotein), O60506 (Heterogeneous nuclear ribonucleoprotein Q), P31153 (S-adenosylmethionine synthase isoform type-2), and P46777 (60S ribosomal protein L5). A total of 652 proteins have been identified as not significantly upregulated or downregulated in the comparison analysis. These proteins did not exhibit statistically significant differences in expression between the compared groups or conditions.

The direction of the contrast model determines the change in log-fold change (logFC) values. For instance, in the depicted figure, P68133 (Actin, alpha skeletal muscle) shows an increased expression of 0.25 (25%) in HIV_noMetS macrophages compared to HC macrophages. It's important to note that the logFC value changes by multiplication with -1 when the direction of the contrast model is reversed.

To account for potential batch effects, the batch factor was included as a cofactor in the model, ensuring that any observed differential expression is not confounded by batch variation.

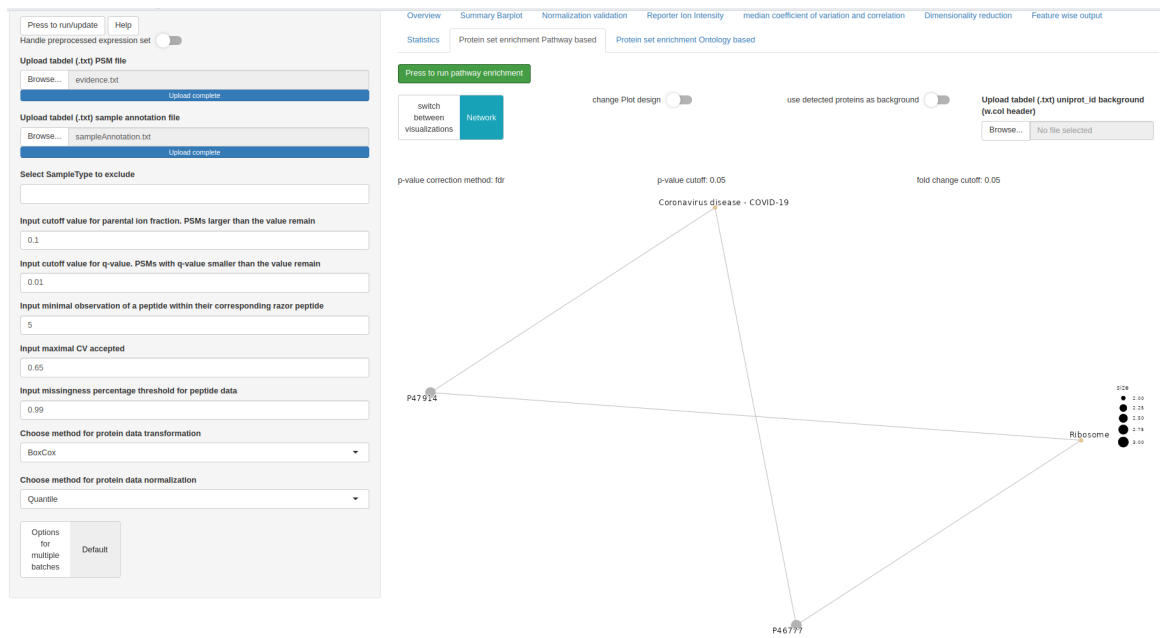


Figure 23: Pathway enrichment. Networkplot indicating the association of differentially expressed proteins with pathways

The pathway enrichment mapped and tested with the exact Fisher test (Sprent 2011) the differentially expressed proteins P46777 (60S ribosomal protein L5) and P47914 (60S ribosomal protein L29) to the ribosome and coronavirus disease (COVID-19) nodes.

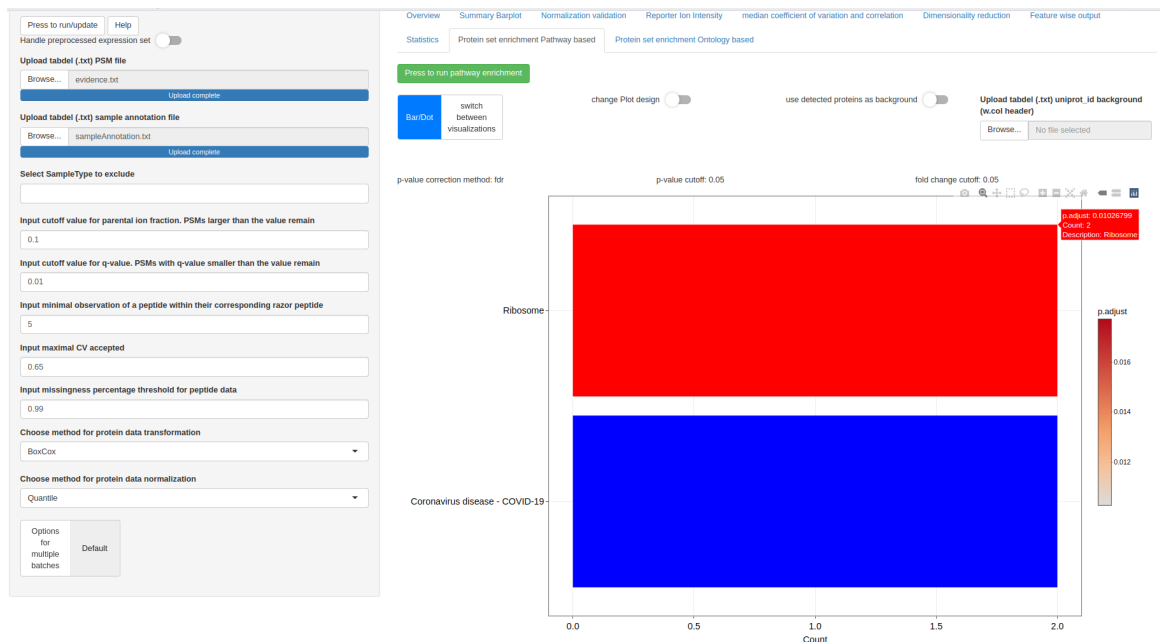


Figure 24: Pathway enrichment. Barplot indicating the interaction significance of differentially expressed proteins

The barplot shows the significance of the two nodes. The count indicates how many proteins are associated with the node of the network. When hovering over the bar the user can read the p-value of the performed Fisher test. The background for the statistical test can be chosen as genome wide (default) or as the detected proteins. When choosing the detected proteins as a background no pathway could be considered as statistically significant.

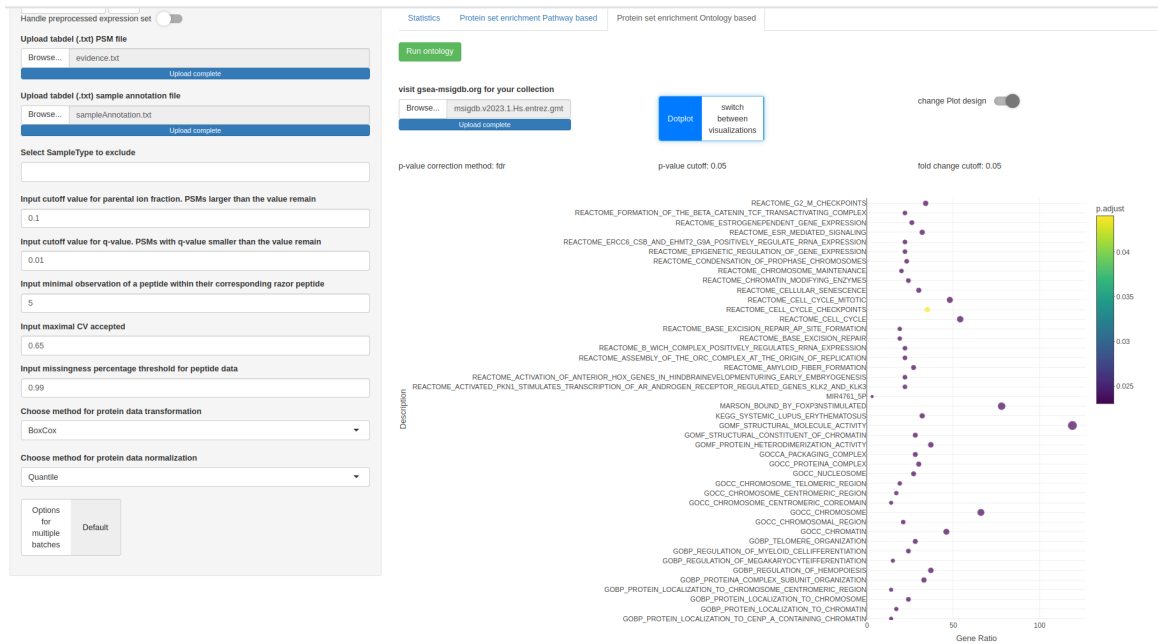


Figure 25: Gene ontology enrichment against the complete human proteome. Snapshot dotplot indicating the interaction significance of found proteins

The position of the dot shows the number of matches for the particular protein set. Colors indicate for the significance level. In this analysis the entire repertoire of detected proteins was used and fetched against the bundle containing all Human gene sets in the Human Molecular Signatures Database (MSigDB). After a runtime of 3 minutes 672 of 24667 gene sets were found significantly over represented. Only the protein set collections with the most protein matches were used (snipping tool Plotly).

4 Discussion

The Proteomics Workbench interface and the ProteoScanR pipeline demonstrated how interactive engagement with the data not only enhances the experience of biologists but also improves the comprehension of the underlying significance of a biological dataset. By utilizing an entropy-based visualization approach, the conservation of information can be validated, allowing users to select appropriate methods and adjust thresholds, cutoffs, and techniques accordingly. With the selection of factors to indicate over multiple plots, biases can be identified on various levels. Additionally, the analysis can be examined on an individual protein basis, enabling the identification of suspicious results. The statistics module provides users with a simple tool to assess and visualize the results, offering clarity to dense scatter plots through hover functions. Enrichment mapping links statistically significant proteins to either the KEGG pathway database or individual research data sets, depending on user selection. These final results place the data in a biological context, which can be explored interactively in graphical visualizations.

4.1 Interactive pipeline

Linear programming scripts are widely utilized for data analysis, and R-shiny provides an efficient platform for implementing these scripts in applications. This approach not only benefits scientists who are not proficient in programming, but it is also convenient for programmers. The Proteomics Workbench user interface offers a visually appealing design, and the interactive menus enhance the user experience by eliminating the need to search for specific lines of code on a black screen. Modifying parameters of functions becomes effortless, and data can be visualized without rerunning the entire script. R-shiny executes functions on demand, which means that graphics, variables, and data frames are not recalculated if their dependencies remain unchanged. This feature makes the application both cost-effective and time-efficient. The analysis pathway is visualized through multiple components, providing users with a comprehensive view of the data. The overview plot, generated using the Q-feature object-oriented programming in the scp R library (Vanderaa & Gatto 2021), serves as a visual representation of the analysis process. This plot allows users to track the progression of the analysis and identify any missing files or samples.

4.2 Mutual Information

Information theory and the concept of mutual information provide a framework for understanding the conservation of entropy in a dataset. Traditionally, the validation of data transformation and normalization methods has been limited to observing distributions through histograms or Quantile-Quantile plots. However, the developed approach goes beyond these conventional methods, providing a deeper context for the variation in the data. By allowing users to choose the method that preserves the maximum amount of information, the approach enables researchers to extract the most valuable insights from their experiments. Normalization methods play a crucial role in data analysis, and their selection depends on the nature of the data and the specific analysis objectives. The mutual information analysis revealed that quantile normalization exhibited the smallest loss of entropy compared to other normalization methods

4.3 Reporter ion intensity

MS2 reporter ion intensities can be effectively visualized using a boxplot, where the medians represent the intensity distribution across various factors such as sample type, batch, or channel. This visualization aids users in assessing the variation and potential biases in the dataset. During the example analysis, the reporter ion intensity plot revealed inconsistencies in the dataset based on signal intensities associated with different batches. It was observed that certain runs exhibited a wide spread of signal intensities, which could indicate technical issues or batch-related variations. These inconsistencies were partly filtered out during the quality control process to ensure the reliability and accuracy of the data.

4.4 Median coefficient of variation

The median coefficient of variation (CV) was calculated for a razor protein in relation to its ambiguous peptides. This statistical parameter measures the variability of the razor protein's abundance across different peptide measurements. The results were then visualized using a boxplot, allowing users to assess the distribution of CV values based on a selected factor. During testing and fine-tuning, the number of observations for ambiguously matched peptides was adjusted to evaluate its impact on the CV. By varying the number of observations, researchers could determine the optimal parameter that yielded meaningful CV values. In this context, the reference values from the SCoPE2 publication (Specht et al. 2021) were employed as benchmarks and subjected to validation. The results showed that using a number of observations of 5 for leading razor peptides was suitable

for identifying a cutoff value of 0.65. This cutoff value was determined by observing the whiskers of the boxplots. By setting this threshold, noisy peptides in the dataset could be effectively reduced, enhancing the quality and reliability of the data.

4.5 Feature-wise plot

The feature-wise output plays a crucial role in enhancing the analysis pathway by offering users the ability to select specific proteins and explore their associated peptide spectra, peptide values, and protein values throughout the analysis. This feature provides a detailed and comprehensive view of the analysis results, enabling users to identify any missing or erroneous data points, particularly in channels with low or high abundance. By examining these individual protein profiles, users can assess the quality of the wet lab work and detect any potential errors or inconsistencies. In the case of observing the abundance of the protein P61313 (60S ribosomal protein L15) over the entire course of the experiment, it becomes apparent that there are missing values within certain runs and channels. Specifically, 14 runs exhibit no signal for this protein. This observation underscores the significance of aggregating data at the peptide and protein levels and combining individual runs to construct the final protein expression set. The scattering of dots in the plot indicates the inflation of small values and the deflation of large values after transformation. The scatter plot of quantile normalized values demonstrates the processing steps taken while preserving outliers and maintaining the biological relevance of the data. This processing steps aid in achieving a more balanced distribution of data and avoids the distortion of biological meaning.

4.6 Statistics module

The statistics module within the application provides users with a user-friendly interface for hypothesis testing, even without prior expertise in statistics. By leveraging the powerful R-package limma (Ritchie et al. 2015), the module offers robust statistical analysis methods, empowering users to perform tests and obtain results to validate their hypotheses. One key feature of the statistics module is its ability to handle multiple factors and therefore correct for batch effects. Users can extend the statistical analysis across various factors, allowing them to quantify the impact of different variables and identify differentially expressed proteins. To enhance the user experience, the visualization of statistical results has been improved, resulting in visually appealing and interactive displays. These visualizations enable users to explore and interpret the results effortlessly, aiding in the comprehension of the statistical findings. By providing intuitive and engaging visual

representations, the module facilitates the understanding and communication of complex statistical analyses. When comparing the group HIV without metabolic syndrome and the healthy control 6 proteins could be found as differentially expressed after correcting the p-values by false discovery rate (FDR (Benjamini & Hochberg 1995)). For example, the protein P68133 (Actin, alpha skeletal muscle) exhibits a log fold change (logFC) of -0.25, indicating a significant decrease in actin levels within the HIV group. This finding aligns with previous publications suggesting that HIV exploits cellular skeleton proteins and alters their expression levels (Turville 2018). By inducing orchestrated structural changes in compartments composed of actin filaments, the virus facilitates its spread and infects other lymphocytes (Rodrigues et al. 2022). Another protein of interest, P47914 (60S ribosomal protein L29), demonstrates the impact of viral infection on protein synthesis. Differential expression of this protein further highlights the perturbations in cellular processes caused by the virus.

4.7 Enrichment

The enrichment analysis module within the application addresses the challenge of selecting protein sets for mapping by incorporating a database-fetching functionality. This feature streamlines the enrichment analysis process and eliminates the need for users to manually select sets to map proteins against. The first variant of the enrichment analysis module utilizes the KEGG database, which offers a comprehensive collection of pathways and their interactions. By accessing this database, users can gain valuable insights into the underlying pathways and their relationships. This automated mapping against the KEGG database provides a convenient and efficient way to perform enrichment analysis. The second variant of the module caters to sophisticated users who may have specific protein sets in mind based on their research question. This flexibility allows users to select and incorporate their own protein sets into the analysis, enabling research in multiple contexts and providing a comprehensive insight into the dataset. Both variants of the enrichment analysis module present the results in interactive plots, offering users a dynamic and immersive experience with the data. Users can explore the enriched pathways and interact with the visualizations, gaining a deeper understanding of the relationships and connections within the dataset. Additionally, if desired, users can generate static plots and download them for use in presentations or other offline contexts. As indicated by the statistical findings, the KEGG enrichment analysis identified proteins associated with the ribosome and COVID-19. Both protein sets were connected to two ribosomal proteins, namely P47914 (60S ribosomal protein L29) and P46777 (60S ribosomal protein L5). These findings align with the fact that HIV and COVID-19, like all known viruses, depend entirely on the host cell's translation machinery for protein synthesis. This includes utilizing the host's ribosomes, tRNAs,

amino acids, and all necessary factors for protein synthesis initiation, elongation, and termination (Ohlmann et al. 2014). Consequently, it is not surprising that these ribosomal proteins were found to be abundant in HIV-infected individuals.

4.8 Limitations

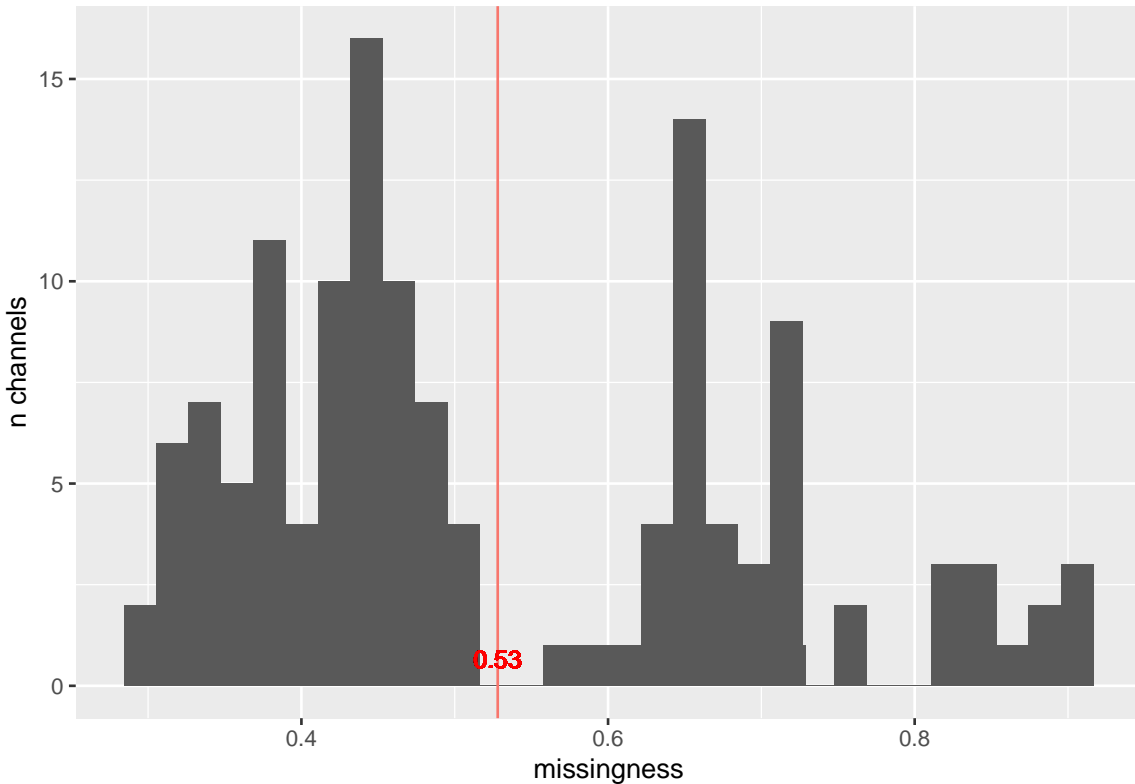


Figure 26: Missingness over channels. Y-axis: Height of the histogram bars show number of channels. X-axis: fraction of missing values. Red line: Mean of number of missing values over all runs

Unfortunately, a substantial number of individual proteins in the data set (totaling 658) have missing values. On average, this amounts to approximately 53% of the proteins across all runs and channels. This situation leads to the need for missing value imputation using techniques such as k-nearest neighbor (K-NN), which can result in averaged results. Additionally, it is important to note that this imputation process can introduce potential loss of power in subsequent statistical analysis. To improve future experiments, it is recommended to increase the number of proteins in the carrier proteome. By expanding the repertoire of proteins included in the carrier proteome, it can enhance the coverage and depth of analysis, providing a more comprehensive understanding of the biological system under investigation. This can potentially lead to more robust and accurate results in downstream analyses.

4.9 Future perspectives

4.9.1 Clustering for stratification of cells.

The advantage of performing single-cell analysis lies in its ability to provide a fine resolution of cellular differences. Unfortunately variation causing effects such as cellular differentiation stages, are mainly unknown when starting single-cell experiments. The next steps in the development of the program aim to enable the stratification of single-cell data sets. The analysis typically begins by finding clusters within the datasets, identifying differentially expressed proteins, and annotating cell types based on their expression profiles. Subsequently, the analysis aims to distinguish sample types based on their expression profiles.

Here I will explain how the analysis could start and elaborate the limitations and challenges for this approach. Additional processing steps will be included after the existing pipeline, so ProteoScanR provides a starting point for further analysis.

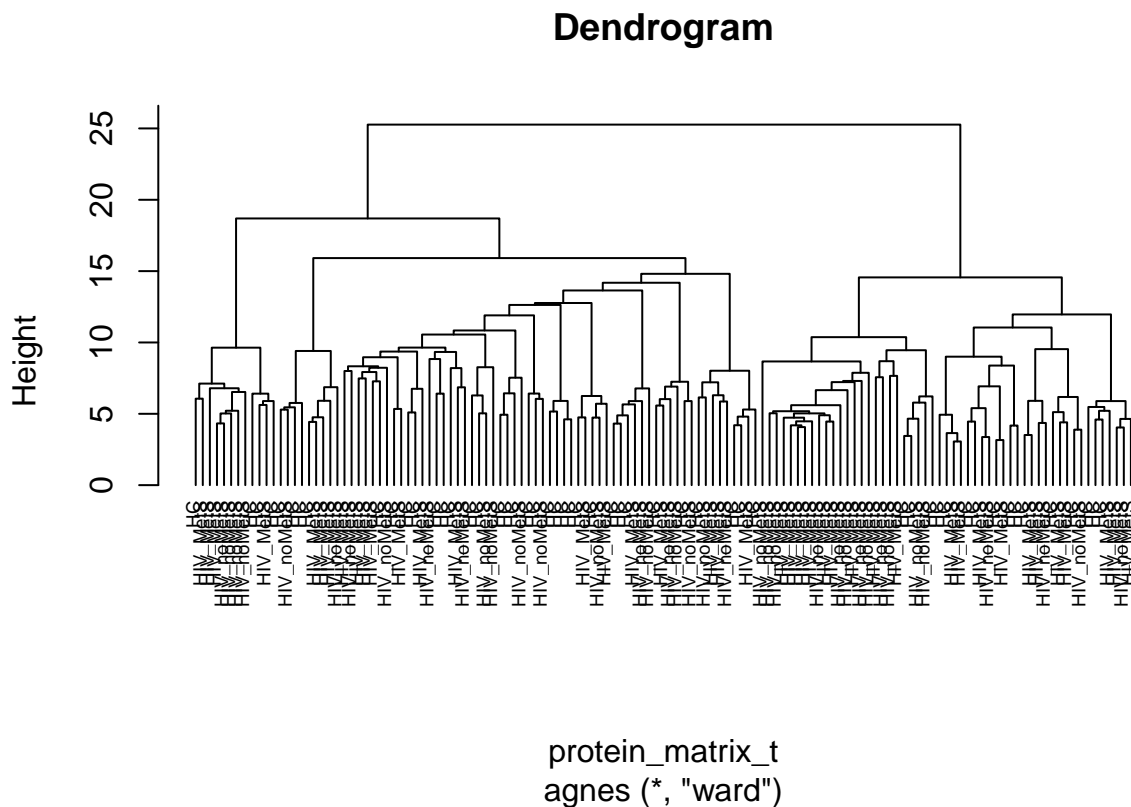


Figure 27: Dendrogram showing the similarity over sample types. Tree was created using Ward's minimum variance method.

As observed in the dendrogram, it is evident that sample type alone does not account for the

variation observed in the data. The branching patterns in the dendrogram suggest that other factors might be significant for contributing to the averaging of protein expression levels. This can potentially lead to a decrease in the statistical power of tests aimed at detecting differential expression between sample types. Ideally, clustering approaches should result in individual clusters that capture distinct sample types, enabling the testing of differential expression within each cluster. This stratification of samples within clusters allows for the identification of unique expression patterns associated with specific biological variations. The dendrogram, as demonstrated above, is an example of hierarchical clustering, which provides a visual representation of the clustering results. In this context, users should have the flexibility to select the desired number of clusters that best explain the underlying biological variation in their dataset. This allows for a more targeted and precise analysis of differential expression within each cluster, facilitating the identification of biologically meaningful patterns and insights. To begin with the k-means clustering approach, it is crucial to determine the optimal number of clusters before conducting the analysis. This can be achieved using various approaches, one of which is the gap statistic method (Tibshirani et al. 2001).

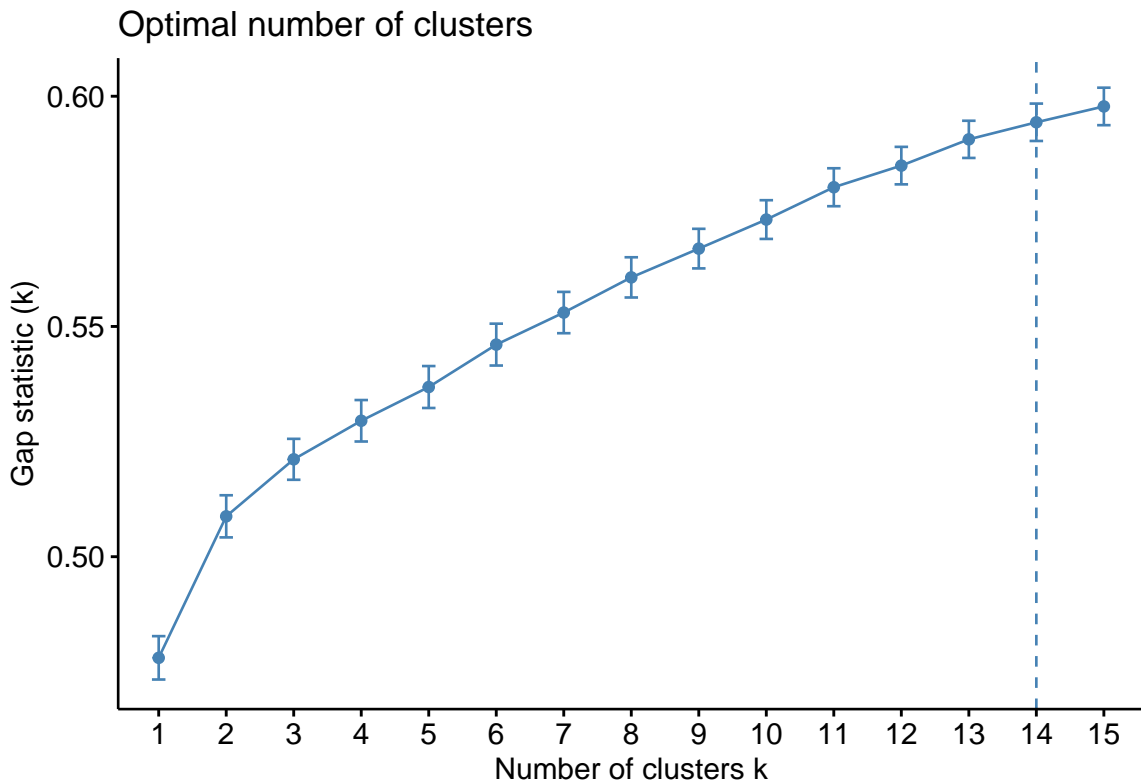


Figure 28: Optimal numbers of clusters calculated with gap statistics method

The gap statistic compares the total intracluster variation across various values of k (number of clusters) to the expected variation under a null reference distribution. The null reference distribution

represents a scenario where no clear clustering patterns exist in the data. However as seen in the gap statistic a high number of clusters will be difficult to distinguish from each other and explore the biological meaning such as differentiation in the example macrophage dataset. Another approach used to determine the optimal number of clusters is the silhouette method.

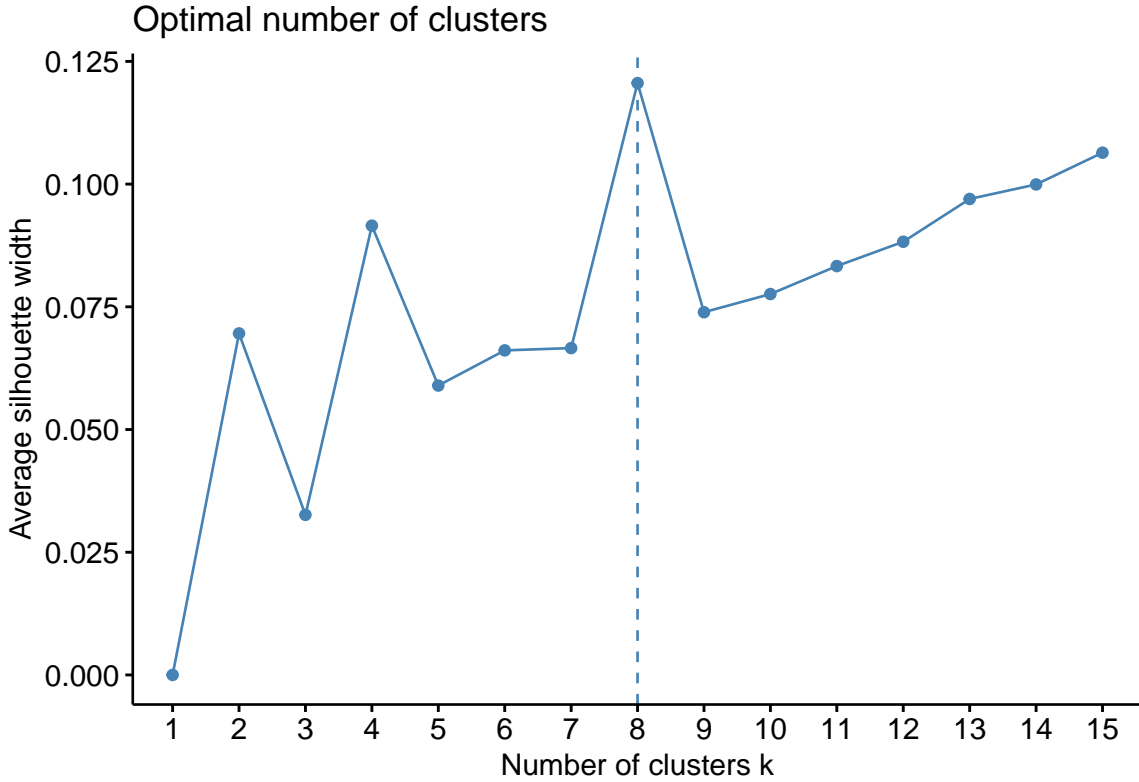


Figure 29: Optimal number of clusters calculated with silhouette method.

The silhouette method calculates silhouette coefficients for each data point, which quantify how closely the point resembles its own cluster compared to other clusters. If the overall distances between clusters are small, indicating overlapping or unclear separation, it is suggested to take the minimum k . This suggests that the data points may not be well-separated into distinct clusters. As suggested by the silhouette method in this case a lower number of clusters to differentiate cell types is recommended.

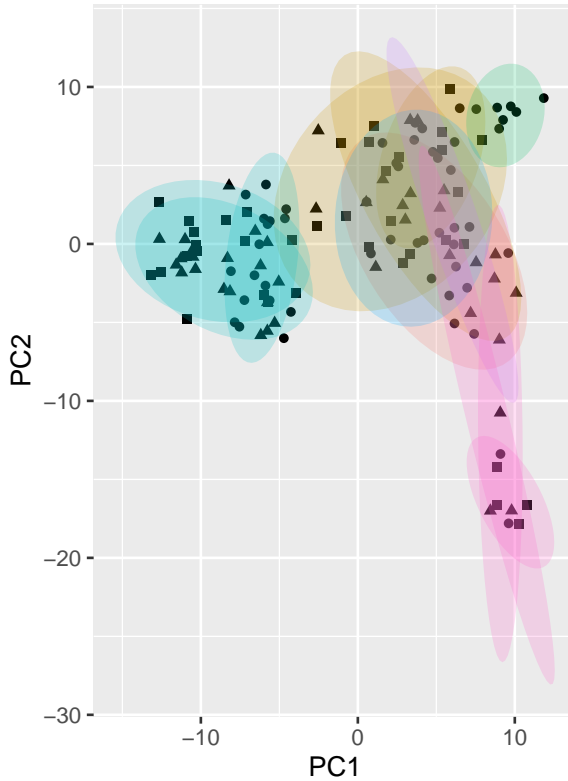


Figure 30: PCA plot with cluster indication. Shape of the datapoints indicate sample types. Clusters are encircled and color coded.

As seen in the principal components analysis, clusters are densely packed, and the plot shows no clear differentiation between the 8 suggested clusters. The dense packing and poor resolution indicates that other factors may be influencing the lack of distinct separation. One of the other factors involves the large number of imputed values due the high rate of missing values in the protein expression set. K-NN is not able to impute biological differences and therefore averages the particular missing value by its k neighbors.

This suggests the utilization of a different data set for developing the clustering module of the future program. By employing a data set with a lower rate of missing values in the protein expression set, the accuracy and reliability of the clustering analysis can be enhanced. Having a data set with less missing data will allow for a more precise identification of clusters and differentiation between cell types.

4.9.2 Machine learning

One potential target for future research could involve leveraging artificial intelligence techniques to predict cellular behavior, cell types, or even diseases. By running the application on a server and

creating a database, it would be possible to harness the power of AI algorithms such as decision trees, random forests, or support vector machines. Applying artificial intelligence to biological data has the potential to enhance the classification of cell types, similar to the earlier discussed clustering approach. However, it is important to note that training and validating these algorithms typically requires supervision and can be a time-consuming task.

Another area of focus, not limited to research topics, could be to enhance the usability of the application. While a development time of 5 months for the pipeline and user interface is sufficient to meet the analytical needs, there is always room for improvement in terms of user-friendliness. It is essential to consider the needs of all users, including the least experienced user. To prevent program crashes and errors, it may be necessary to implement try-catch around code blocks, as well as validate-need statements for the validation of user input. Additionally, creating a user-friendly environment involves establishing effective channels of communication between users and developers, such as utilizing platforms like GitHub for collaboration and feedback.

5 Conclusion

Through this project, I demonstrated that computational analysis can be made accessible to a wide range of biologists by providing an interactive environment. It is important to recognize that there cannot be a one-size-fits-all approach for proteomics datasets. Therefore, the application offers easy-to-interpret visualizations that allow users to assess the patterns and trends in their observed datasets. The default options provided in the application are based on successful analysis pipelines such as ScoPE2 (Specht et al. 2021), serving as a starting point for customization at multiple levels.

The example dataset provided showcases the inherent challenges in proteomic data analysis. It exhibits skewed distributions, batch effects, and a substantial number of missing values. Despite these complexities, the ProteoScanR pipeline and Proteomics Workbench interface offer biologists a convenient means to address their research questions and validate the computations performed. The example use case also sheds light on the fact that previous proteomics publications, such as the ScoPE2 study (Specht et al. 2021), may not always employ the gold standard in data processing. This emphasizes the importance of critically evaluating and refining data processing steps through trial and error to achieve optimal results. The interactive environment provided by the application allows users to navigate the trial and error process without experiencing frustration. This user-friendly interface ensures that researchers can iteratively refine their data processing steps and analyze the results in a seamless manner. Furthermore, the scalability of the application was initially unknown until the final submission of the single-cell dataset. The programming and testing of the application primarily focused on bulk datasets, typically consisting of up to four runs at once. However, it is noteworthy that the application demonstrates remarkable efficiency and performance, even when running large datasets. The ability of the application to efficiently handle larger datasets, such as single-cell studies, is a significant advantage. It allows researchers to analyze complex and extensive datasets without sacrificing performance or compromising the quality of the results. This scalability makes the application a valuable tool for analyzing diverse types of biological data, accommodating the needs of researchers working with both smaller and larger datasets.

ProteoScanR pipeline and Proteomics Workbench user interface serve as valuable tools for individual researchers and research communities, enabling them to analyze and visualize their data in meetings, even on non-performant computers. However, one of the future perspectives involves deploying the application on a server, making it accessible to research groups around the world. This would enhance collaboration and facilitate the sharing of insights and findings across different geographical locations. By providing a centralized platform for proteomics analysis, aiming to foster scientific

advancements and enable researchers to make significant contributions to their respective fields. Furthermore by having a central hub for proteomic data analysis and the use of artificial intelligence the biological meaning could be brought to a wider context. Since proteomic data could be saved without violating data protection laws, algorithms could be employed to learn from large datasets.

An important aspect of learning from the data involves annotating specimens, particularly in the context of single-cell proteomics. The clustering approach is a primary focus for future development and analysis in the near term. By employing clustering algorithms and stratifying the data, individual cells can be labeled and annotated based on their phenotypes. This annotation process involves associating protein sets collections with specific clusters or cell types, providing a more comprehensive understanding of cellular heterogeneity and functional characteristics.

In conclusion, the ProteoScanR pipeline and Proteomics Workbench interface provide a user-friendly and efficient approach for proteomic data analysis, enabling biologists to address their research questions and validate computations. Future perspectives include deploying the application on a server for global accessibility, leveraging artificial intelligence techniques, and implementing clustering approaches to further enhance annotation and understanding of cellular heterogeneity and functional characteristics.

6 Bibliography

- A., K. & Demmers, J. A. A. (2012), *Labeling Methods in Mass Spectrometry Based Quantitative Proteomics*, InTech.
- Aebersold, R. & Mann, M. (2003), ‘Mass spectrometry-based proteomics’, *Nature* **422**, 198–207.
- Bacharach, M. (1965), ‘Estimating nonnegative matrices from marginal data’, *International Economic Review* **6**, 294.
- Beltran, P. M. J., Federspiel, J. D., Sheng, X. & Cristea, I. M. (2017), ‘Proteomics and integrative omic approaches for understanding host-pathogen interactions and infectious diseases’, *Molecular Systems Biology* **13**, 922.
- Benjamini, Y. & Hochberg, Y. (1995), ‘Controlling the false discovery rate: A practical and powerful approach to multiple testing’, *Journal of the Royal Statistical Society: Series B (Methodological)* **57**, 289–300.
- Benjamini, Y. & Yekutieli, D. (2001), ‘The control of the false discovery rate in multiple testing under dependency’, *The Annals of Statistics* **29**.
- Brownridge, P. & Beynon, R. J. (2011), ‘The importance of the digest: Proteolysis and absolute quantification in proteomics’, *Methods* **54**, 351–360.
- Budnik, B., Levy, E., Harmange, G. & Slavov, N. (2018), ‘Scope-ms: mass spectrometry of single mammalian cells quantifies proteome heterogeneity during cell differentiation’, *Genome Biology* **19**, 161.
- Cobb, M. (2017), ‘60 years ago, francis crick changed the logic of biology’, *PLOS Biology* **15**, e2003243.
- Cox, J. & Mann, M. (2008), ‘Maxquant enables high peptide identification rates, individualized p.p.b.-range mass accuracies and proteome-wide protein quantification’, *Nature Biotechnology* **26**, 1367–1372.
- Cox, J., Neuhauser, N., Michalski, A., Scheltema, R. A., Olsen, J. V. & Mann, M. (2011), ‘Andromeda: A peptide search engine integrated into the maxquant environment’, *Journal of Proteome Research* **10**, 1794–1805.

- Fang, P., Li, X., Dai, J., Cole, L., Camacho, J. A., Zhang, Y., Ji, Y., Wang, J., Yang, X.-F. & Wang, H. (2018), 'Immune cell subset differentiation and tissue inflammation', *Journal of Hematology & Oncology* **11**, 97.
- Gygi, S. P., Rochon, Y., Franzia, B. R. & Aebersold, R. (1999), 'Correlation between protein and mRNA abundance in yeast', *Molecular and Cellular Biology* **19**, 1720–1730.
- Holm, S. (1979), 'A simple sequentially rejective multiple test procedure', *Scandinavian Journal of Statistics* **6**, 65–70.
- Houtven, J. V., Hooyberghs, J., Laukens, K. & Valkenborg, D. (2021), 'Constand: An efficient normalization method for relative quantification in small- and large-scale omics experiments in r bioconductor and python', *Journal of Proteome Research* **20**, 2151–2156.
- Iribarne, J. V. (1976), 'On the evaporation of small ions from charged droplets', *The Journal of Chemical Physics* **64**, 2287.
- Johnson, W. E., Li, C. & Rabinovic, A. (2007), 'Adjusting batch effects in microarray expression data using empirical bayes methods', *Biostatistics* **8**, 118–127.
- Karahalil, B. (2016), 'Overview of systems biology and omics technologies', *Current Medicinal Chemistry* **23**, 4221–4230.
- Kullback, S. & Leibler, R. A. (1951), 'On information and sufficiency', *The Annals of Mathematical Statistics* **22**, 79–86.
- Kwon, Y. W., Jo, H.-S., Bae, S., Seo, Y., Song, P., Song, M. & Yoon, J. H. (2021), 'Application of proteomics in cancer: Recent trends and approaches for biomarkers discovery', *Frontiers in Medicine* **8**.
- Lan, L., Djuric, N., Guo, Y. & Vucetic, S. (2013), 'Ms-k nn: protein function prediction by integrating multiple data sources', *BMC Bioinformatics* **14**, S8.
- Leek, J. T., Johnson, W. E., Parker, H. S., Jaffe, A. E. & Storey, J. D. (2012), 'The <tt>sva</tt> package for removing batch effects and other unwanted variation in high-throughput experiments', *Bioinformatics* **28**, 882–883.
- Liou, Y.-R., Wang, Y.-H., Lee, C.-Y. & Li, P.-C. (2015), 'Buoyancy-activated cell sorting using targeted biotinylated albumin microbubbles', *PLOS ONE* **10**, e0125036.

- Maes, E., Cools, N., Willems, H. & Baggerman, G. (2020), ‘Facs-based proteomics enables profiling of proteins in rare cell populations’, *International Journal of Molecular Sciences* **21**, 6557.
- Maes, E., Hadiwikarta, W. W., Mertens, I., Baggerman, G., Hooyberghs, J. & Valkenborg, D. (2016), ‘Constand : A normalization method for isobaric labeled spectra by constrained optimization’, *Molecular & Cellular Proteomics* **15**, 2779–2790.
- Magnusson, R., Rundquist, O., Kim, M. J., Hellberg, S., Na, C. H., Benson, M., Gomez-Cabrero, D., Kockum, I., Tegnér, J. N., Piehl, F., Jagodic, M., Mellergård, J., Altafini, C., Ernerudh, J., Jenmalm, M. C., Nestor, C. E., Kim, M.-S. & Gustafsson, M. (2022), ‘Rna-sequencing and mass-spectrometry proteomic time-series analysis of t-cell differentiation identified multiple splice variants models that predicted validated protein biomarkers in inflammatory diseases’, *Frontiers in Molecular Biosciences* **9**.
- Marx, V. (2019), ‘A dream of single-cell proteomics’, *Nature Methods* **16**, 809–812.
- McCarthy, D. J., Campbell, K. R., Lun, A. T. L. & Wills, Q. F. (2017), ‘Scater: pre-processing, quality control, normalization and visualization of single-cell rna-seq data in r’, *Bioinformatics* **33**, 1179–1186.
- McInnes, L., Healy, J. & Melville, J. (2018), ‘Umap: Uniform manifold approximation and projection for dimension reduction’.
- Minakshi, P., Kumar, R., Ghosh, M., Saini, H. M., Ranjan, K., Brar, B. & Prasad, G. (2019), *Single-Cell Proteomics: Technology and Applications*, Elsevier.
- Nygaard, V., Rødland, E. A. & Hovig, E. (2016), ‘Methods that remove batch effects while retaining group differences may lead to exaggerated confidence in downstream analyses’, *Biostatistics* **17**, 29–39.
- Ohlmann, T., Mengardi, C. & López-Lastra, M. (2014), ‘Translation initiation of the hiv-1 mrna’, *Translation* **2**, e960242.
- Parker, C. E., Warren, M. R. & Mocanu, V. (2010), *Mass Spectrometry for Proteomics*.
- Pearson, K. (1900), ‘X. *i*on the criterion that a given system of deviations from the probable in the case of a correlated system of variables is such that it can be reasonably supposed to have arisen from random sampling</i>’, *The London, Edinburgh, and Dublin Philosophical Magazine and Journal of Science* **50**, 157–175.

- Petelski, A. A., Emmott, E., Leduc, A., Huffman, R. G., Specht, H., Perlman, D. H. & Slavov, N. (2021), ‘Multiplexed single-cell proteomics using scope2’, *Nature Protocols* **16**, 5398–5425.
- Philpott, M. K., Stanciu, C. E., Kwon, Y. J., Bustamante, E. E., Greenspoon, S. A. & Ehrhardt, C. J. (2017), ‘Analysis of cellular autofluorescence in touch samples by flow cytometry: implications for front end separation of trace mixture evidence’, *Analytical and Bioanalytical Chemistry* **409**, 4167–4179.
- Phipson, B., Lee, S., Majewski, I. J., Alexander, W. S. & Smyth, G. K. (2016), ‘Robust hyperparameter estimation protects against hypervariable genes and improves power to detect differential expression’, *The Annals of Applied Statistics* **10**.
- Pitt, J. J. (2009), ‘Principles and applications of liquid chromatography-mass spectrometry in clinical biochemistry’, *The Clinical biochemist. Reviews* **30**, 19–34.
- Ritchie, M. E., Phipson, B., Wu, D., Hu, Y., Law, C. W., Shi, W. & Smyth, G. K. (2015), ‘limma powers differential expression analyses for rna-sequencing and microarray studies’, *Nucleic Acids Research* **43**, e47–e47.
- Rodrigues, V., Taheraly, S., Maurin, M., San-Roman, M., Granier, E., Hanouna, A. & Benaroch, P. (2022), ‘Release of hiv-1 particles from macrophages is promoted by an anchored cytoskeleton and driven by mechanical constraints’, *Journal of Cell Science* **135**.
- Sakia, R. M. (1992), ‘The box-cox transformation technique: A review’, *The Statistician* **41**, 169.
- Schoof, E. M., Furtwängler, B., Üresin, N., Rapin, N., Savickas, S., Gentil, C., Lechman, E., auf dem Keller, U., Dick, J. E. & Porse, B. T. (2021), ‘Quantitative single-cell proteomics as a tool to characterize cellular hierarchies’, *Nature Communications* **12**, 3341.
- Senko, M. W., Beu, S. C. & McLaffertycor, F. W. (1995), ‘Determination of monoisotopic masses and ion populations for large biomolecules from resolved isotopic distributions’, *Journal of the American Society for Mass Spectrometry* **6**, 229–233.
- Smyth, G. K. (2004), ‘Linear models and empirical bayes methods for assessing differential expression in microarray experiments’, *Statistical Applications in Genetics and Molecular Biology* **3**, 1–25.
- Specht, H., Emmott, E., Petelski, A. A., Huffman, R. G., Perlman, D. H., Serra, M., Kharchenko, P., Koller, A. & Slavov, N. (2021), ‘Single-cell proteomic and transcriptomic analysis of macrophage heterogeneity using scope2’, *Genome Biology* **22**, 50.

- Sprent, P. (2011), *Fisher Exact Test*, Springer Berlin Heidelberg.
- Sutermaster, B. A. & Darling, E. M. (2019), ‘Considerations for high-yield, high-throughput cell enrichment: fluorescence versus magnetic sorting’, *Scientific Reports* **9**, 227.
- TANAKA, K. (2009), ‘The proteasome: Overview of structure and functions’, *Proceedings of the Japan Academy, Series B* **85**, 12–36.
- Tannous, A., Boonen, M., Zheng, H., Zhao, C., Germain, C. J., Moore, D. F., Sleat, D. E., Jadot, M. & Lobel, P. (2020), ‘Comparative analysis of quantitative mass spectrometric methods for subcellular proteomics’, *Journal of Proteome Research* **19**, 1718–1730.
- Tibshirani, R., Walther, G. & Hastie, T. (2001), ‘Estimating the number of clusters in a data set via the gap statistic’, *Journal of the Royal Statistical Society Series B: Statistical Methodology* **63**, 411–423.
- Turville, S. (2018), ‘All-round manipulation of the actin cytoskeleton by hiv’, *Viruses* **10**, 63.
- Vanderaa, C. & Gatto, L. (2021), ‘Replication of single-cell proteomics data reveals important computational challenges’, *Expert Review of Proteomics* **18**, 835–843.
- Väremo, L., Nielsen, J. & Nookaew, I. (2013), ‘Enriching the gene set analysis of genome-wide data by incorporating directionality of gene expression and combining statistical hypotheses and methods’, *Nucleic Acids Research* **41**, 4378–4391.
- Wang, Y., Luo, W. & Reiser, G. (2008), ‘Trypsin and trypsin-like proteases in the brain: Proteolysis and cellular functions’, *Cellular and Molecular Life Sciences* **65**, 237–252.
- Wang, Z., Gerstein, M. & Snyder, M. (2009), ‘Rna-seq: a revolutionary tool for transcriptomics’, *Nature Reviews Genetics* **10**, 57–63.
- Wilm, M. (2011), ‘Principles of electrospray ionization’, *Molecular & Cellular Proteomics* **10**, M111.009407.
- Wilschefski, S. & Baxter, M. (2019), ‘Inductively coupled plasma mass spectrometry: Introduction to analytical aspects’, *Clinical Biochemist Reviews* **40**, 115–133.
- Wu, T., Hu, E., Xu, S., Chen, M., Guo, P., Dai, Z., Feng, T., Zhou, L., Tang, W., Zhan, L., Fu, X., Liu, S., Bo, X. & Yu, G. (2021), ‘clusterprofiler 4.0: A universal enrichment tool for interpreting omics data’, *The Innovation* **2**, 100141.

Ye, Z., Batth, T. S., Rüther, P. & Olsen, J. V. (2022), ‘A deeper look at carrier proteome effects for single-cell proteomics’, *Communications Biology* **5**, 150.

Zhao, Y., Wong, L. & Goh, W. W. B. (2020), ‘How to do quantile normalization correctly for gene expression data analyses’, *Scientific Reports* **10**, 15534.

Ünige A. Laskay, Lobas, A. A., Srzentić, K., Gorshkov, M. V. & Tsybin, Y. O. (2013), ‘Proteome digestion specificity analysis for rational design of extended bottom-up and middle-down proteomics experiments’, *Journal of Proteome Research* **12**, 5558–5569.

7 Appendix

7.1 Wet lab

7.1.1 Cells sorting protocol

1. 96 single cells from each donor were sorted into a single plate. Each well contained a single cell.
As such, 12 different plates containing single cells from 12 different donors were prepared.
2. Carrier plates were also prepared. In the carrier plates, 100 cells from one donor were sorted into each well. 24 such wells (3 columns) were prepared for each donor.

7.1.2 Digestion protocol

1. Prepare 25 ng/ μ L trypsin in 100 mmol/L Triethylammonium bicarbonate buffer (TEAB).
2. Add 25 ng/ μ L trypsin: 2 μ L to the carrier samples, 1 μ L to the single cell samples.
3. Seal the plates.
4. Centrifuge (2 min at 120 G).
5. Incubate overnight at 37 °C.

7.1.3 Labeling protocol

1. Let the TMTpro labels come to room temperature so that all the condensation on the tube is gone. Dissolve the TMTpro reagents in anhydrous acetonitril (ACN) to obtain a concentration of 10 μ g/ μ L.
2. Add 1 μ L of TMTpro reagents according to the tables. For one set of plates, you will need 16 μ L of each label. It is recommended to aliquot a slightly larger volume, around 20 μ L.
3. Seal the plates.
4. Centrifuge for 2 minutes at 120 G.
5. Incubate for 1 hour at room temperature.
6. Prepare a 5

7. Add 1 μ L of the 5
8. Seal the plates.
9. Centrifuge for 2 minutes at 120 G.
10. Incubate for 1 hour at room temperature.
11. Cover the plates with cap strips.

7.1.4 Pooling protocol

1. Wash a 10 μ L glass microsyringe five times with ACN.
2. Use the microsyringe to combine TMTpro-labeled samples into 36 LC autosampler vials with built-in glass inserts.
3. Combine six carrier wells from each sample and add the carrier proteome to the 36 TMTpro sets.
4. Combine the first set by taking well A1 from the first single-cell plate, well A2 from the second plate, well A3 from the third plate, and so on. For the next set, take well A1 from the second plate, well A2 from the third plate, and so on. Combine 12 sets following this scheme. Combine the next 24 sets by following the same scheme for rows B and C.
5. Vacuum centrifuge the combined sets to dryness.
6. Dissolve the dried samples in 7 μ L of buffer A and transfer them to LC-MS/MS for further analysis.

7.2 Dry lab

7.2.1 R-version info

```
## R version 4.3.0 (2023-04-21)
## Platform: x86_64-pc-linux-gnu (64-bit)
## Running under: Ubuntu 22.04.2 LTS
##
## Matrix products: default
## BLAS: /usr/lib/x86_64-linux-gnu/blas/libblas.so.3.10.0
```

```

## LAPACK: /usr/lib/x86_64-linux-gnu/lapack/liblapack.so.3.10.0

##
## locale:
## [1] LC_CTYPE=en_US.UTF-8      LC_NUMERIC=C
## [3] LC_TIME=de_AT.UTF-8       LC_COLLATE=en_US.UTF-8
## [5] LC_MONETARY=de_AT.UTF-8   LC_MESSAGES=en_US.UTF-8
## [7] LC_PAPER=de_AT.UTF-8      LC_NAME=C
## [9] LC_ADDRESS=C               LC_TELEPHONE=C
## [11] LC_MEASUREMENT=de_AT.UTF-8 LC_IDENTIFICATION=C
##
## time zone: Europe/Vienna
## tzcode source: system (glibc)
##
## attached base packages:
## [1] parallel  stats4    grid      stats     graphics grDevices utils
## [8] datasets  methods   base
##
## other attached packages:
## [1] visNetwork_2.1.2           snowfall_1.84-6.2
## [3] snow_0.4-4                 piano_2.16.0
## [5] org.Hs.eg.db_3.17.0        AnnotationDbi_1.62.1
## [7] infotheo_1.2.0.1          clusterProfiler_4.8.1
## [9] plotly_4.10.1              spsComps_0.3.2.1
## [11] DT_0.28                   shinydashboard_0.7.2
## [13] shinyWidgets_0.7.6         shiny_1.7.4
## [15] cluster_2.1.4             factoextra_1.0.7
## [17] tibble_3.2.1              sva_3.48.0
## [19] BiocParallel_1.34.2        genefilter_1.82.1
## [21] mgcv_1.8-42                nlme_3.1-162
## [23] impute_1.74.1             CONSTAND_1.8.0
## [25] limma_3.56.1              scater_1.28.0
## [27] scuttle_1.10.1            reshape2_1.4.4
## [29] dplyr_1.1.2                ggplot2_3.4.2

```

```

## [31] SingleCellExperiment_1.22.0 scp_1.10.0
## [33] QFeatures_1.10.0           MultiAssayExperiment_1.26.0
## [35] SummarizedExperiment_1.30.1 Biobase_2.60.0
## [37] GenomicRanges_1.52.0       GenomeInfoDb_1.36.0
## [39] IRanges_2.34.0            S4Vectors_0.38.1
## [41] BiocGenerics_0.46.0       MatrixGenerics_1.12.0
## [43] matrixStats_0.63.0        magrittr_2.0.3
## [45] glue_1.6.2                Gmisc_3.0.2
## [47] htmlTable_2.4.1           Rcpp_1.0.10
## [49] DiagrammeR_1.0.10         tinytex_0.45
##
## loaded via a namespace (and not attached):
## [1] ProtGenerics_1.32.0          bitops_1.0-7
## [3] enrichplot_1.20.0           lubridate_1.9.2
## [5] HDO.db_0.99.1              httr_1.4.6
## [7] RColorBrewer_1.1-3          tools_4.3.0
## [9] backports_1.4.1             utf8_1.2.3
## [11] R6_2.5.1                  lazyeval_0.2.2
## [13] withr_2.5.0                gridExtra_2.3
## [15] cli_3.6.1                 shinyjs_2.1.0
## [17] scatterpie_0.2.0            slam_0.1-50
## [19] labeling_0.4.2              sass_0.4.6
## [21] yulab.utils_0.0.6           gson_0.1.0
## [23] foreign_0.8-84              DOSE_3.26.1
## [25] rstudioapi_0.14             RSQLite_2.3.1
## [27] gridGraphics_0.5-1           generics_0.1.3
## [29] gtools_3.9.4                car_3.1-2
## [31] GO.db_3.17.0                Matrix_1.5-4.1
## [33] ggbeeswarm_0.7.2            fansi_1.0.4
## [35] abind_1.4-5                 lifecycle_1.0.3
## [37] yaml_2.3.7                  edgeR_3.42.2
## [39] carData_3.0-5                shinytoastr_2.1.1
## [41] gplots_3.1.3                 qvalue_2.32.0

```

```
## [43] blob_1.2.4                  promises_1.2.0.1
## [45] crayon_1.5.2                 lattice_0.21-8
## [47] beachmat_2.16.0               cowplot_1.1.1
## [49] annotate_1.78.0               KEGGREST_1.40.0
## [51] pillar_1.9.0                  knitr_1.43
## [53] fgsea_1.26.0                 marray_1.78.0
## [55] codetools_0.2-19              fastmatch_1.1-3
## [57] downloader_0.4                gggfun_0.0.9
## [59] data.table_1.14.8              treeio_1.24.0
## [61] vctrs_0.6.2                  png_0.1-8
## [63] gtable_0.3.3                 assertthat_0.2.1
## [65] cachem_1.0.8                 xfun_0.39
## [67] S4Arrays_1.0.4                mime_0.12
## [69] tidygraph_1.2.3               survival_3.5-5
## [71] sets_1.0-24                  ellipsis_0.3.2
## [73] ggtree_3.8.0                 bit64_4.0.5
## [75] bslib_0.4.2                  irlba_2.3.5.1
## [77] KernSmooth_2.23-21            vigor_0.4.5
## [79] rpart_4.1.19                 colorspace_2.1-0
## [81] DBI_1.1.3                     Hmisc_5.1-0
## [83] nnet_7.3-19                   tidyselect_1.2.0
## [85] bit_4.0.5                     compiler_4.3.0
## [87] BiocNeighbors_1.18.0            DelayedArray_0.26.3
## [89] shadowtext_0.1.2               caTools_1.18.2
## [91] checkmate_2.2.0                scales_1.2.1
## [93] relations_0.6-13              stringr_1.5.0
## [95] digest_0.6.31                 rmarkdown_2.21
## [97] XVector_0.40.0                htmltools_0.5.5
## [99] pkgconfig_2.0.3                base64enc_0.1-3
## [101] sparseMatrixStats_1.12.0      fastmap_1.1.1
## [103] rlang_1.1.1                   htmlwidgets_1.6.2
## [105] DelayedMatrixStats_1.22.0     farver_2.1.1
## [107] jquerylib_0.1.4              jsonlite_1.8.4
```

```
## [109] GOSemSim_2.26.0           BiocSingular_1.16.0
## [111] RCurl_1.98-1.12            Formula_1.2-5
## [113] GenomeInfoDbData_1.2.10   ggplotify_0.1.0
## [115] patchwork_1.1.2            munsell_0.5.0
## [117] ape_5.7-1                  viridis_0.6.3
## [119] MsCoreUtils_1.12.0         stringi_1.7.12
## [121] ggraph_2.1.0               zlibbioc_1.46.0
## [123] MASS_7.3-60                plyr_1.8.8
## [125] ggrepel_0.9.3              Biostrings_2.68.1
## [127] graphlayouts_1.0.0          splines_4.3.0
## [129] locfit_1.5-9.7              igraph_1.4.3
## [131] ggpubr_0.6.0                ggsignif_0.6.4
## [133] ScaledMatrix_1.8.1          XML_3.99-0.14
## [135] evaluate_0.21               tweenr_2.0.2
## [137] httpuv_1.6.11              tidyrr_1.3.0
## [139] purrrr_1.0.1                polyclip_1.10-4
## [141] clue_0.3-64                 BiocBaseUtils_1.2.0
## [143] ggforce_0.4.1               rsvd_1.0.5
## [145] broom_1.0.4                 xtable_1.8-4
## [147] AnnotationFilter_1.24.0     tidytree_0.4.2
## [149] rstatix_0.7.2               later_1.3.1
## [151] viridisLite_0.4.2            aplot_0.1.10
## [153] forestplot_3.1.1             memoise_2.0.1
## [155] beeswarm_0.4.0               timechange_0.2.0
## [157] shinyAce_0.4.2
```

List of Figures

1	Flowchart presenting the processing by ProteoScanR	14
2	Summary showing the process of the analysis pipeline	31
3	Barchart showing the number of peptide spectrum matches, peptides and proteins	32
4	Mutual information with default setting	33
5	Popup showing the dependencies for the CONSTANd normalization	34
6	Mutual information with quantile normalization	35
7	Reporter ion intensity with selection on channel. The selected factor will be highlighted and indicated in the legend.	36
8	Reporter ion intensity with selection on file	37
9	Reporter ion intensity with selection on samptype	38
10	Median covariance of razor proteins with selection on samptype	39
11	Median coefficient of variation (CV) of leading razor proteins per cell with selection on Raw.file	40
12	Median coefficient of variation (CV) of leading razor proteins calculated for 2 observations per cell, with selection on Raw.file	41
13	Median coefficient of variation (CV) of leading razor proteins calculated for 10 observations per cell, with selection on Raw.file	42
14	Correlation heatmap	43
15	Dimensionality reduction analysis depicting sample types (indicated by shape) and raw files (indicated by color). Top: principle component analysis (PCA). Lower: Uniform Manifold Approximation and Projection (UMAP)	44
16	Dimensionality reduction analysis showcasing sample types (represented by shape) and raw files (represented by color). Top: Principal Component Analysis (PCA). Bottom: Uniform Manifold Approximation and Projection (UMAP). For the UMAP visualization, the k value for the NN-descent algorithm was modified to 15.	45
17	3D visualization of dimensionality reduction analysis showcasing sample types (represented by shape) and raw files (represented by color). Top: Principal Component Analysis (PCA). Bottom: Uniform Manifold Approximation and Projection (UMAP)	46

18	Batch corrected dimensionality reduction analysis showcasing sample types (represented by shape) and raw files (represented by color). upper top: Principal Component Analysis (PCA). upper bottom: Uniform Manifold Approximation and Projection (UMAP). lower top: 3D Principal Component Analysis (PCA). lower bottom: 3D Uniform Manifold Approximation and Projection (UMAP)	47
19	Batch corrected dimensionality reduction analysis showcasing sample types (represented by shape) and raw files (represented by color). upper top: Principal Component Analysis (PCA). upper bottom: Uniform Manifold Approximation and Projection (UMAP). lower top: 3D Principal Component Analysis (PCA). lower bottom: 3D Uniform Manifold Approximation and Projection (UMAP)	48
20	Feature wise output for the protein P61313 (=60S ribosomal protein L15) over the course of the pipeline.	49
21	Popup window for checking the dependency of the statistic module	50
22	Statistic module	51
23	Pathway enrichment. Networkplot indicating the association of differentially expressed proteins with pathways	53
24	Pathway enrichment. Barplot indicating the interaction significance of differentially expressed proteins	54
25	Gene ontology enrichment against the complete human proteome. Snapshot dotplot indicating the interaction significance of found proteins	55
26	Missingness over channels. Y-axis: Height of the histogram bars show number of channels. X-axis: fraction of missing values. Red line: Mean of number of missing values over all runs	60
27	Dendrogram showing the similarity over sample types. Tree was created using Ward's minimum variance method.	61
28	Optimal numbers of clusters calculated with gap statistics method	62
29	Optimal number of clusters calculated with silhouette method.	63
30	PCA plot with cluster indication. Shape of the datapoints indicate sample types. Clusters are encircled and color coded.	64